Chapter 3: Elucidation of a low spin cobalt(II) system in a distorted tetrahedral geometry

Credit should be given to the following people for their work that appears in this chapter. M. J. Allen first synthesized the [PhBP$_3$]Co-X (X = I, Br, or Cl) complexes and structurally characterized them. A. J. Di Bilio helped with the EPR measurements.

3.1 Introduction

Metal centers that reside in unusual coordination geometries sometimes display unique physical properties that correlate to novel modes of chemical reactivity.[1] Metalloenzymes can exploit subtle structure/function relationships to achieve specific catalytic transformations by intimately tuning the local stereochemistry and ligand-field in a protein active site. An appreciation of specific ligand-to-metal interactions in protein active sites is therefore highly dependent on our basic understanding of elementary stereochemical and ligand-field relationships in coordination chemistry.[2] Moreover, our community's general desire to make use of these elementary principles to rationally design catalysts selective for specific transformations motivates ongoing interest in this area.[3,4] We suggest that coupling (i) an axial distortion in a pseudotetrahedral cobalt(II) complex of approximate threefold symmetry with (ii) a strong ligand-field donor strength can provide access to a doublet rather than a quartet electronic ground state. This result is of interest because, to the best of our knowledge, all previously characterized four-coordinate cobalt(II) systems that are low spin have adopted approximate square planar structure types.[5,6] Owing to its historically well-behaved and rich spectroscopy, there has been longstanding interest in using cobalt(II) substitution to probe local stereochemical environments in the active sites of native enzymes. Perhaps the most familiar example of this use is that of zinc carbonic anhydrase.[7] Establishing that pseudotetrahedral cobalt(II) can exhibit spectroscopic features consistent with a doublet rather than a quartet ground state is particularly interesting in this latter context.

The series of paramagnetic cobalt complexes described below is well suited to probing the ligand-field donor strength that is imposed by the tris(phosphino)borate

ligand [PhB(CH$_2$PPh$_2$)$_3$]$^-$, abbreviated throughout as [PhBP$_3$].[8,9] The [PhBP$_3$] ligand[10] is a structurally similar but anionic relative to the well-known tris(phosphine) ligand[11,12] H$_3$CC(CH$_2$PPh$_2$)$_3$ (abbreviated herein as triphos[13]) that was originally reported by Hewertson and Watson in 1964.[14] Our continued focus on developing neutral complexes that feature a partially insulated borate counteranion, fixed at a short but remote distance from a transition metal that is coordinated by neutral amine or phosphine donor arms, is in part due to the promise these formal zwitterions hold for catalytic applications.[15,16] Studying the elementary and catalytic reaction processes of zwitterions of this type, and comparing their reactivity to isostructural but more conventional cationic relatives, is paramount to defining the role zwitterionic systems might offer to homogeneous catalysis. It is also of interest to examine the impact that the fastened borate unit can have upon the intimate electronic structure of the coordinated metal center. This study describes our initial efforts to address this latter issue. We provide evidence to show that, when coordinated to a cobalt(II) ion, the [PhBP$_3$] anion provides access to a unique low spin cobalt(II) complex, [PhBP$_3$]CoI (**3.1**), whose stereochemical structure is best regarded as distorted tetrahedral. Given the intense spectroscopic and magnetic scrutiny divalent cobalt has received during the past several decades,[17,18] elucidation of this low spin system is particularly interesting. Complex **3.1** and its chloride and bromide relatives are structurally related to the well-known, but cationic, triphos supported cobalt(II) systems popularized by Sacconi and more recently by Huttner.[19,20] The data presented herein afford a first comparative glance at the dramatic electronic consequences that arise when the borate counteranion is embedded within the phosphine donor ligand framework.

The synthetic, structural, and spectroscopic data for the title complex **3.1** are presented below to corroborate its low spin assignment. Two related low spin cobalt(II) derivatives, ([PhBP$_3$]Co^{II}X) (X = Br (**3.2**), Cl (**3.3**)), are also described. These latter two complexes feature an added complexity in that they are dimeric in the solid-state, but predominantly monomeric in solution. The collection of comparative solid-state and solution EPR spectra for **3.1**, **3.2**, and **3.3** is presented. For comparison, structural and spectroscopic data for a high spin derivative that was obtained directly from **3.1** is also described.

3.2 Results

3.2.1 Synthesis and solid-state structures of ([PhBP$_3$]Co^{II}X) (X = I, Br, Cl)

Eq. 3.1 and Eq. 3.2 present the synthesis of the three halide derivatives ([PhBP$_3$]Co^{II}X) (X = I, Br, Cl). The high yield synthesis of the iodide complex [PhBP$_3$]CoI, (**3.1**), derived from the thallium reagent [PhBP$_3$]Tl, has been previously described. Although the bromide and chloride derivatives could be similarly prepared, they were best derived metathetically from the iodide complex: in situ iodide abstraction by TlPF$_6$ in THF, followed by addition of KBr or NaCl, converted [PhBP$_3$]CoI to ([PhBP$_3$]Co(μ-Br))$_2$, (**3.2**), and ([PhBP$_3$]Co(μ-Cl))$_2$, (**3.3**), respectively. Complexes **3.2** and **3.3** were isolated in yields typically greater than 80% when the metathesis protocol was repeated twice prior to workup. The halide derivatives **3.1**, **3.2**, and **3.3** gave rise to distinct and well-resolved, though paramagnetically shifted, ^{1}H NMR spectra.
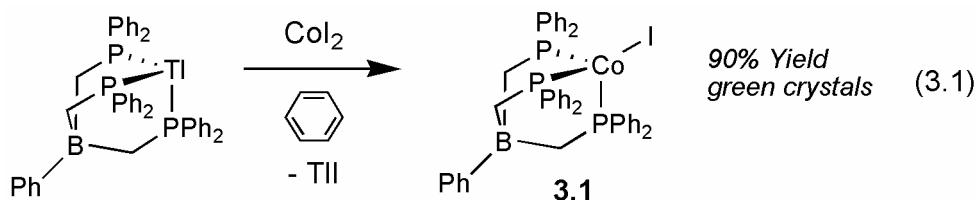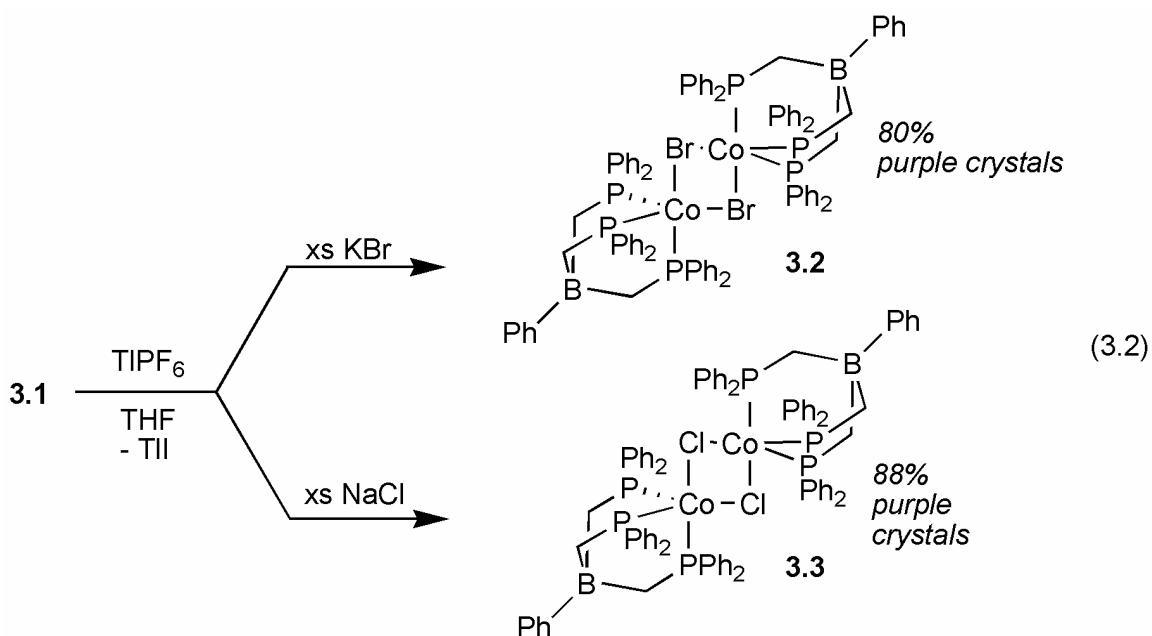
The iodide complex **3.1** is green whereas the chloride and bromide complexes **3.2** and **3.3** are purple in the crystalline state. This difference in color between polycrystalline samples of the three complexes correlates with their solid-state structures, which were determined by low temperature X-ray diffraction studies. Displacement ellipsoid representations for the solid-state structures (collected at 98 K) of **3.1**, **3.2**, and **3.3** are depicted in Figure 3.1, 3.2, and 3.3, respectively. The structure shown to the right for each complex provides a simplified representation in which the aryl carbon atoms from the diphenylphosphine donors have been omitted. Furthermore, the structures on the right of the bromide and chloride derivatives are rotated so that the bridging halide ligands are eclipsed. Only the bridged halide protruding out of the plane of the page is visible.
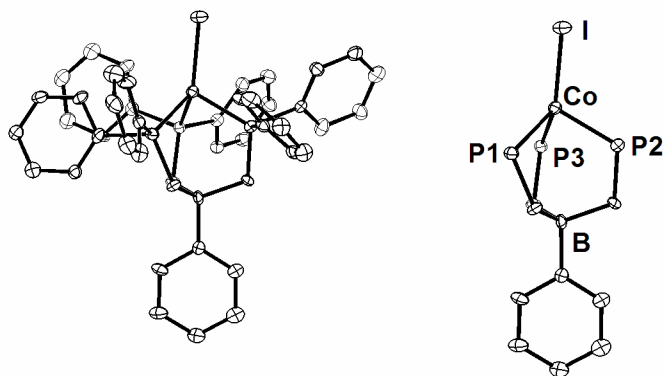
Figure 3.1. Displacement ellipsoids are represented at 50%. The structure on the right is shown without aryl carbon atoms for clarity. Selected interatomic distances (Å) and angles (deg) for [PhBP$_3$]CoI, (**3.1**): Co1-P1, 2.200(2); Co1-P2, 2.206(2); Co1-P3, 2.282(2); Co1-I1, 2.488(1); Co1-B1, 3.490(8). P1-Co1-P2, 90.33(8); P1-Co1-P3, 94.46(7); P2-Co1-P3, 91.95(7); P1-Co1-I1, 117.54(6); P2-Co1-I1, 129.19(6); P3-Co1-I1, 124.01(6).

Most striking in Figure 3.1 is the monomeric structure obtained for the iodide complex **3.1** in comparison to the dimeric solid-state structures obtained for the bromide and chloride complexes **3.2** and **3.3**, respectively. Although none of the three complexes adopts an idealized local geometry, they can be approximated as structure types typical of cobalt(II). The iodide **3.1** has pseudotetrahedral coordination, with low formal symmetry due to a strong axial distortion and inequivalent Co-phosphine bond lengths and angles. By contrast, the bromide and chloride derivatives can be regarded as square pyramidal structures at the localized cobalt center of each respective dimeric unit. In each of the three structures, the tridentate [PhBP$_3$] ligand exhibits two short and one modestly elongated Co-P bond. The P-Co-P angles vary only slightly from 90°.
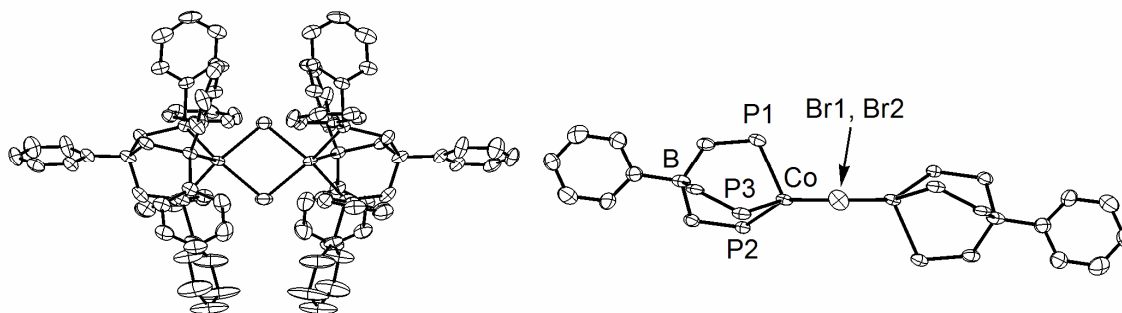
Figure 3.2. Displacement ellipsoids are represented at 50%. The structure on the right is shown without aryl carbon atoms for clarity, and the dimer is rotated such that the bridging halide ligands are eclipsed. Selected interatomic distances (Å) and angles (deg) for ([PhBP$_3$]Co(μ-Br))$_2$ (**3.2**): Co1-Co1(#1), 3.668(1); Co1-P3, 2.235(2); Co1-P2, 2.247(2); Co1-P1, 2.336(2); Co1-Br1, 2.413(1); Co1-Br2, 2.424(1); Co1-B1, 3.570(6). Co1-Br1-Co1(#1), 98.97(5); Co1-Br2-Co1(#1), 98.37(5); P2-Co1-P3, 87.42(6); P1-Co1-P3, 92.35(6); P1-Co1-P2, 93.44(6); P3-Co1-Br1, 165.70(5); P2-Co1-Br1, 93.63(5); P1-Co1-Br1, 101.81(4); P3-Co1-Br2, 91.35(5); P2-Co1-Br2, 153.37(5); P1-Co1-Br2, 113.19(4); Br1-Co1-Br2, 81.33(3). Symmetry transformations used to generate equivalent atoms: #1 - x, y, -z + 1/2.

The bromide complex **3.2** features a rigorously planar Co$_2$Br$_2$ rhombus that is bisected by a crystallographic C_2-axis running through the two bromide ligands. The C_2-axis effectively places the elongated axial Co-P bonds on opposite faces of the Co$_2$Br$_2$ plane. By comparison, the Co$_2$Cl$_2$ unit of the chloride complex **3.3** gently buckles from planarity. The two elongated, axial Co-P bonds in this case reside on the same face of the Co$_2$Cl$_2$ unit. The gentle buckling in **3.3**, along with the decreased size of the chloride bridge, effectively slides the two cobalt centers closer together by comparison to their

distance in **3.2** (3.668(1) Å in **3.2** versus 3.497(1) Å in **3.3**). Dimeric **3.3** is structurally

very similar to its dicationic relative [((triphos)Co(μ-Cl))$_2$][BPh$_4$]$_2$: the Co-Co distance in

[((triphos)Co(μ-Cl))$_2$][BPh$_4$]$_2$ is 3.52 Å, and its Co-Cl-Co angle is 100.0°, to be compared

with an average Co-Cl-Co angle of 98.2° in **3.3**.[19c,20] The solid-state structure of

[((triphos)Co(μ-OH))$_2$][BPh$_4$]$_2$ has also been determined and is similarly dimeric, though

the O-Co-O angles are much smaller and average 69.5°.[19c] Spectroscopic data confirms

that the bromide derivative [((triphos)Co(μ-Br))$_2$][BPh$_4$]$_2$ is dimeric as well;[19c] its

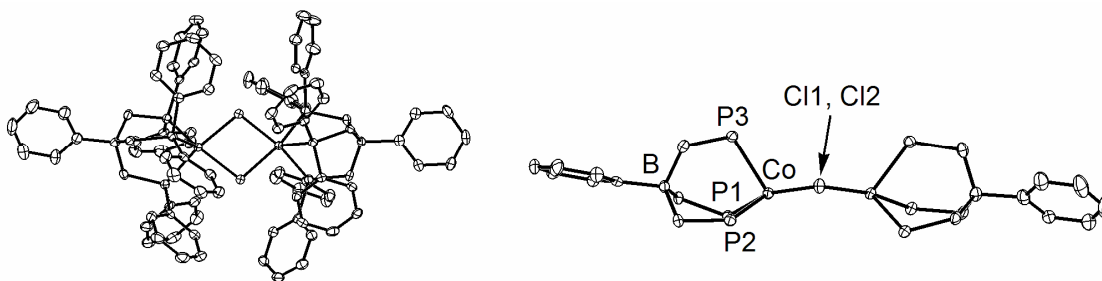solid-state crystal structure has not yet been reported.

Figure 3.3. Displacement ellipsoids are represented at 50%. The structure on the right is shown without aryl carbon atoms for clarity, and the dimer is rotated such that the bridging halide ligands are eclipsed. Selected interatomic distances (Å) and angles (deg) for ([PhBP$_3$]Co(μ-Cl))$_2$ (**3.3**): Co1-Co2, 3.497(1); Co1-B1, 3.551(3); Co2-B2, 3.598(3); Co1-P1, 2.224(1); Co1-P2, 2.244(1); Co1-P3, 2.391(1); Co1-Cl1, 2.284(1); Co1-Cl2, 2.321(1); Co2-P4, 2.227(1); Co2-P5, 2.239(1); Co2-P6, 2.336(1); Co2-Cl1, 2.314(1); Co2-Cl2, 2.332(1). Co1-Cl1-Co2, 99.02(3); Co1-Cl2-Co2, 97.46(3); P1-Co1-P2, 88.16(3); P1-Co1-Cl1, 162.76(3); P2-Co1-Cl1, 92.82(3); P1-Co1-Cl2, 92.55(3); P2-Co1-Cl2, 159.70(3); Cl1-Co1-Cl2, 80.65(2); P1-Co1-P3, 91.09(3); P2-Co1-P3, 92.66(3); Cl1-Co1-P3, 106.04(3); Cl2-Co1-P3, 107.60(3); Cl1-Co2-Cl2, 79.79(2).

The solid-state structure of the iodide complex **3.1** exhibits approximate C_s symmetry.[21] An appreciable axial distortion gives rise to I-Co-P bond angles that are much larger than those found in idealized tetrahedral structures (P1-Co1-I1, 117.54(6); P2-Co1-I1, 129.19(6); P3-Co1-I1, 124.01(6)). Complex **3.1** is gently distorted from molecular threefold symmetry by a modest elongation of one of its phosphine donors by comparison to the other two (Co1-P1, 2.200(2); Co1-P2, 2.206(2); Co1-P3, 2.282(2)). Worth noting is that monomeric **3.1** is formally a 15 electron complex; this is very unusual for cobalt(II) systems supported by three phosphine donors. Similar 15 electron, monomeric, and pseudotetrahedral cobalt(II) halides supported by tris(pyrazolyl)- and tris(thioether)borate ligands have been reported previously.[22,23] An attempted synthesis of the analogous "[(triphos)CoI]$^+$" system was reported to have failed due to spontaneous reduction of the cobalt(II) center to cobalt(I).[19c]

3.2.2 Magnetic data (SQUID) for ([PhBP$_3$]Co^{II}X) (X = I, Br, Cl)

The temperature dependence of the magnetic susceptibility for complexes **3.1**, **3.2**, and **3.3** was studied by SQUID magnetometry. Average magnetic moments were adjusted for diamagnetic contributions using Pascal's constants and were fitted in the temperature range specified to use data that obeyed the Curie-Weiss law reasonably well. This was established from χ_m^{-1} versus T plots, which are shown in Figures 3.4B and 3.5B. For each case, the samples studied by SQUID magnetometry had provided satisfactory combustion analyses, as recorded in the Experimental section. These same sample batches were also used to obtain the EPR spectra that are discussed in the following section.
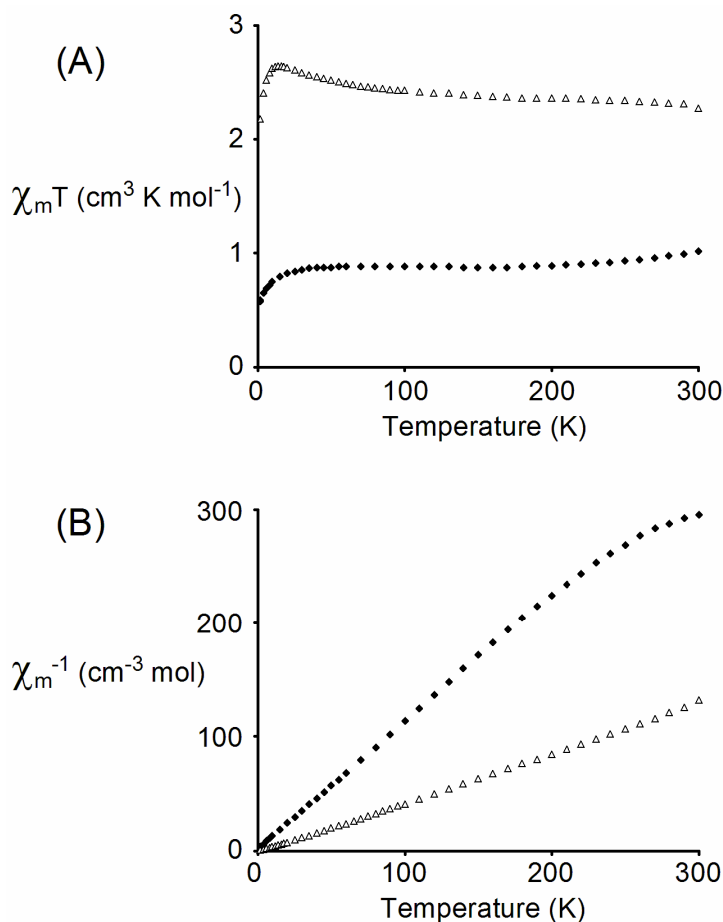
Figure 3.4. (A) SQUID plot of $\chi_m T$ (cm^3 K mol^{-1}) versus T: [PhBP$_3$]CoI, **3.1**, ($\blacklozenge$) and [PhBP$_3$]CoO(2,6-dimethylphenyl), **3.4**, (Δ). (B) SQUID plot of χ_m^{-1} (mol/cm^3) versus T: [PhBP$_3$]CoI, **3.1**, ($\blacklozenge$) and [PhBP$_3$]CoO(2,6-dimethylphenyl), **3.4**, (Δ).

Figure 3.4A displays the temperature dependence of the calculated magnetic moment $\chi_m T$ (see Experimental section for details) for complex **3.1**, and Figure 3.4B plots its χ_m^{-1} versus temperature. The magnetic data for **3.1** is unexpected for a 4-coordinate cobalt(II) system in a pseudo-tetrahedral coordination geometry. Its magnetic moment shows little variation in the temperature range between 30 and 220 K.

The Curie law observed in this range indicates that the doublet state is the only state that is thermally populated. Above 220 K, the effective moment increases, albeit very gradually, possibly suggesting that a high spin state is slightly but increasingly populated as the temperature rises above 220 K. The concentration of a high spin state at the elevated temperatures is very small, however, as even at 300 K the value for χ_mT only reaches 1.01. We note that the gradual rise in the moment that is observed above 220 K for **3.1** was reproducible and does not appear to be an artifact of the experiment. An average magnetic moment of 0.89 cm^3 K mol^{-1} was obtained for **3.1** by fitting the susceptibility data in the temperature range between 10 and 310 K. A fit to the region from 30 to 220 K, where the sample shows good Curie-Weiss behavior, provides an average moment of 0.88. For a 4-coordinate cobalt(II) complex, this moment would typically imply a cobalt(II) ion in an approximate *square planar* geometry.[24] Similar low spin moments are also common for cobalt(II) systems with higher coordination numbers (e.g., square pyramidal, trigonal bipyramidal, or octahedral type structures),[18,25] the value of 0.88 cm^3 K mol^{-1} tending toward the high side of what has been typically observed for low spin cobalt(II). By contrast, magnetic moments for tetrahedral and pseudo-tetrahedral structure types more closely related to [PhBP$_3$]CoI (T_d, C_{3v}, and lower symmetries) typically fall within a range between 2.3 and 3.4 cm^3 K mol^{-1} and are assigned as high spin.[25,26] The average *g* value of 3.06 that is extracted from the SQUID magnetization data, assuming a moment of 2.65 μ_B (χ_mT = 0.88), is much higher than the effective *g* value directly obtained by solid-state EPR spectroscopy ($g \approx 2.1$), as discussed below. The crude relationship between *g* and μ_{eff}, as defined by the simplified equation $\mu_{eff} = g\{S(S + 1)\}^{1/2}$, assumes complete quenching of an orbital contribution,[27] which may be a

serious oversimplification in the present context. The room temperature benzene solution magnetic moment of **3.1** was estimated by the method of Evans and provided a value of 2.87 μ_B, assuming a diamagnetic correction from Pascal's constants, in close agreement with that obtained from the SQUID data at 300 K.[28] We suggest that the solid-state and solution moments are most consistent with a low spin assignment for **3.1**, and that a low spin ground state is very reasonable for a complex of this type based upon the rationale provided in the discussion section. Moreover, the low spin assignment is further corroborated by the EPR data for **3.1**.

The solid-state magnetic susceptibilities for polycrystalline samples of the dimeric bromide ([PhBP$_3$]Co(μ-Br))$_2$ and chloride ([PhBP$_3$]Co(μ-Cl))$_2$ were also measured by SQUID magnetometry and are plotted, *per dimeric unit*, in Figure 3.5. The magnetic data obtained for the dimers are more complex than the data obtained for monomeric **3.1**. Each set of susceptibility data was collected twice to verify its experimental reproducibility. Little, if any, evidence for detectable antiferromagnetic coupling in dimers **3.2** and **3.3** can be gleaned from the temperature-dependent plots of $\chi_m T$ and χ_m^{-1}. The acid test for antiferromagnetic exchange coupling in a dimeric complex consisting of two spin $^1/_2$ ions is that the susceptibility (χ_m) should reach a maximum as the temperature of the sample is lowered, but then fall precipitously to zero as the sample is cooled further. For both **3.2** and **3.3**, the magnetic moments decrease very gently from 310 K down to about 80 K, at which point they level off until reaching the lowest temperature region where intermolecular paramagnetic quenching begins to occur. The expected maximum in the susceptibility for **3.2** and **3.3** is not observed, in contrast to the temperature-dependent susceptibilities Sacconi reported for [((triphos)Co(μ-X))$_2$][BPh$_4$]$_2$

(X = Br, Cl, OH), indicating the dicationic dimers exhibit strong antiferromagnetic coupling (J < -100 cm^{-1}) between their Co^{2+} centers.[19c]
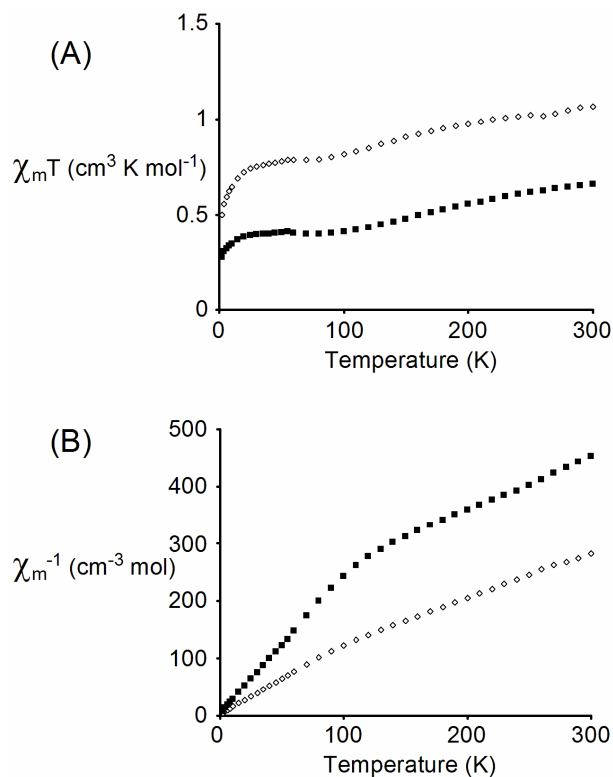

Figure 3.5. (A) SQUID plot of $\chi_m T$ (cm^3 K mol^{-1}) versus T: ([PhBP$_3$]Co(μ-Br))$_2$, **3.2**, (■) and ([PhBP$_3$]Co(μ-Cl))$_2$, **3.3**, (◊). (B) SQUID plot of χ_m^{-1} (mol/cm^3) versus T: ([PhBP$_3$]Co(μ-Br))$_2$, **3.2**, (■) and ([PhBP$_3$]Co(μ-Cl))$_2$, **3.3**, (◊).

Antiferromagnetic exchange behavior is most typical of halide-bridged cobalt(II), copper(II), and titanium(I) dimers, where an unpaired electron resides at each metal center,[29] and it is emphasized that antiferromagnetic exchange does not appear to be present in either **3.2** or **3.3**. The net change in the moment for both **3.2** and **3.3** is rather small between 300 and 80 K. For example, at 300 K the moment of chloride **3.3** is 1.06 cm^3 K mol^{-1}, which decreases to 0.79 at 80 K. For bromide **3.2**, the moment at 300 K

(0.66) is appreciably lower than for **3.3** and only decreases to a value of 0.40 at 80 K. For

a simple ferromagnetic exchange interaction ($J > 0$) between the two spin $^1/_2$ ions in

dimers **3.2** and **3.3**, a plot of $\chi_m T$ versus T is expected to show a rise in the curve as the

temperature is lowered. Instead, we observe a gentle decrease in $\chi_m T$ (and likewise μ_{eff})

as the temperature is lowered, which decreases dramatically only at very low temperature

due to the onset of intermolecular magnetic quenching interactions. A fit of the lower

temperature data, where the Curie-Weiss law is obeyed reasonably well ($T < 110$ K),

provided a magnetic moment 0.40 cm^3 K mol^{-1} and $\theta = -1.48 \pm 0.49$ K for complex **3.2**.

A moment of 0.77 cm^3 K mol^{-1} and theta value of $\theta = -3.13 \pm 0.67$ K was obtained for

complex **3.3** when fit in the same temperature regime. Zero-field splitting, weak

exchange, and mixing of the triplet and singlet states of **3.2** and **3.3** likely complicate the

observed magnetism and contribute to the gradual attenuation rather than rise of the

moment of each sample as the temperature is lowered, as would have been expected for

systems exhibiting pronounced ferromagnetic exchange. Regardless, we suggest that the

magnetic data for **3.2** and **3.3** are most consistent when assigning them to $S = 1$ ground

states. The EPR data for solid samples of **3.2** and **3.3** are also most consistent with a

triplet ground state assignment (see below); the signal amplitude for these dimers

increases as the temperature of each sample is lowered from 25 to 3.6 K, as is to be

expected for a weak ferromagnetically coupled dimer with two $S = ^1/_2$ spin centers.

A dimeric cobalt(II) complex whose magnetism may be related to that observed

for **3.2** and **3.3** was provided by Sacconi and co-workers in 1980.[30] They reported that the

μ-thiolato complex [((triphos)Co(μ-SCH$_3$))$_2$][BPh$_4$]$_2$ provided a μ_{eff} of 1.8 μ_B ($\chi_m T = 0.40$) that gradually decreased to 0.8 μ_B at 130 K, at which point it leveled off down to

the lowest temperature for which data was recorded (87 K). The reasoning Sacconi and co-workers provided to explain the odd magnetic behavior of $[((\text{triphos})\text{Co}(\mu\text{-SCH}_3))_2][\text{BPh}_4]_2$ was that antiferromagnetic exchange occurred between the spin $^1/_2$ cobalt centers through the $\mu\text{-SCH}_3$ units, but that the limiting value represented a contribution from partial occupation of a higher triplet state. In our case, the limiting value at lower temperature represents a triplet state likely mixed with a singlet state that is close in energy.

It should be noted that the difference between the total $\chi_m T$ (and μ_{eff}) for solid samples of **3.2** and **3.3** is not so pronounced in solution. Evans method measurements for **3.2** and **3.3** in benzene-d_6 at 25 °C provided moments of 2.7 μ_B and 3.0 μ_B, respectively, similar to the solution moment obtained for **3.1**.[31] As will be suggested by the EPR data discussed in the following section, these solution moments reflect a change in both geometry and spin state for **3.2** and **3.3** in toluene solution.

3.2.3 EPR spectra for ([PhBP$_3$]Co$^{\text{II}}$X) (X = I, Br, Cl)

The EPR spectra for **3.1**, **3.2**, and **3.3** are extremely sensitive to oxygen due to a high spin impurity that results from a well-defined ligand oxidation process that has been carefully studied for the case of **3.1**. High-quality spectra for all three complexes were only acquired using thoroughly recrystallized samples that afforded satisfactory combustion analysis. The absence of high spin oxidation products was further confirmed by optical spectroscopy prior to EPR data collection.
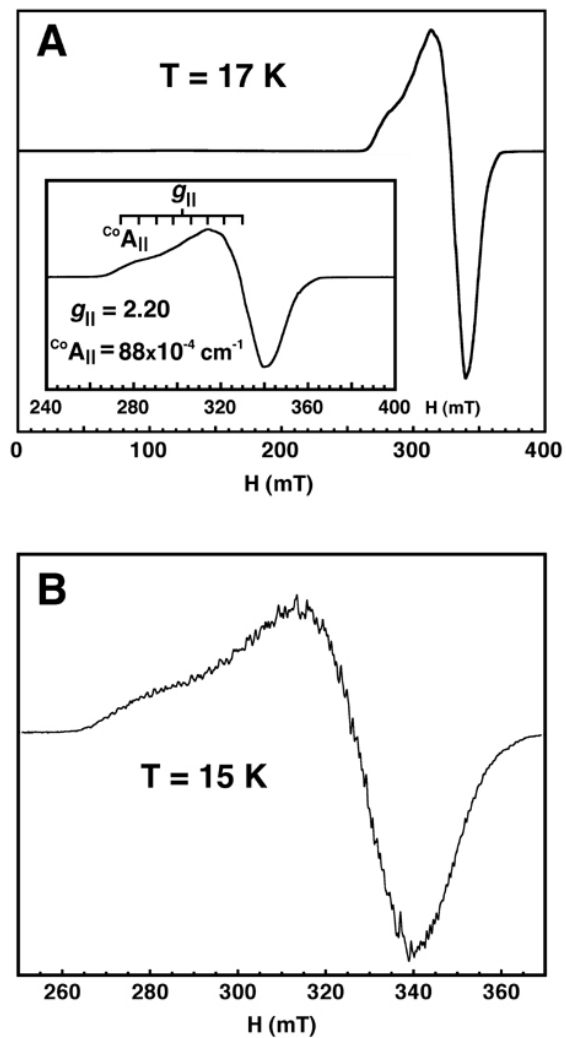
Figure 3.6. (A) EPR spectrum of a glassy toluene solution of [PhBP$_3$]CoI (**3.1**) at 17 K. $g_{\parallel}$ and $A_{\parallel}$ were estimated by simulating the EPR spectrum (inset). (B) EPR spectrum of a glassy toluene solution of [PhBP$_3$]CoI in toluene-d_8 at 15 K. See Experimental section for parameters.

The EPR spectrum in glassy toluene (17 K) of a pure sample of **3.1** is shown in Figure 3.6. Due to the high oxygen sensitivity of **3.1**, the spectra that were originally obtained showed a rather broad feature in the region $g \approx 4.8$ (ca. 120 mT). This feature

was entirely removed upon rigorous exclusion of oxygen from the sample. The broad feature at ~4.8 corresponds to a signal from the high spin complex [PhB(CH$_2$PPh$_2$)(CH$_2$P(O)Ph$_2$)$_2$]CoI (see Experimental section for details). The spectrum of pure **3.1** is nearly independent of temperature (except for its intensity) in the temperature range 20 K to 140 K. It is characterized by an axial g factor ($g_\parallel$ = 2.20 and $g_\perp$ = 2.05) and poorly resolved ^{59}Co (I = 7/2) hyperfine splitting. However, a very complex super-hyperfine splitting pattern was resolved below 50 K in toluene-d_8 (Figure 3.6b),[32] ascribable to the ^{31}P (I = 1/2)[33] and possibly ^{127}I$^-$ (I = 5/2) donor atoms. An isotropic EPR spectrum with g_{iso} = 2.1 was observable at room temperature, further confirming the low spin nature of **3.1**. The powder EPR spectrum of **3.1** shows features analogous to those of the frozen toluene sample. EPR signals for high spin cobalt(II) systems are typically observed only below ~30 K due to the fast spin-lattice relaxation times of the high spin Co(II) nucleus.[34] That we are able to observe an intense signal for **3.1** even at room temperature further supports the notion that **3.1** has a doublet ground state both in solution and in the solid-state.

The solid-state magnetic data that were presented above for **3.2** and **3.3** suggested that they each have triplet ground states close in energy to possibly mixed singlet excited states, and that the magnitude of exchange energy J is difficult to measure from the SQUID data alone. To the extent that ferromagnetic exchange is present, it is likely very small (<10 cm^{-1}). To further explore each of these systems, their EPR spectra were recorded using the same samples that had been carefully purified for the magnetic measurements. As for **3.1**, admission of adventitious oxygen to samples of **3.2** and **3.3** produced oxidation products that afforded spectra with signals centered at $g \approx 4.8$.

Problematic is that these features coincidentally overlap with the low field EPR signal expected (and observed in the solid-state) for the pure dimers of **3.2** and **3.3**. Again, rigorous exclusion of oxygen solved this problem and high quality spectra were obtained. The EPR spectra (Figure 3.7 and 3.9) for pure polycrystalline samples of both **3.2** and **3.3** are well-resolved below 30 K. Each spectrum supports the suggestion of the triplet species at low temperature: the intensity of these spectra were not attenuated, but rather increased, from 25 to 3.6 K, consistent with weak ferromagnetic coupling. The temperature dependence of the solid-state EPR spectrum of **3.2** is shown in Figure 3.8. We attempted to simulate the EPR spectra of the polycrystalline samples of **3.2** and **3.3** under the assumption that the exchange energy $|J| >>$ than the X-band microwave quantum (0.3 cm^{-1}). In such cases the triplet state can be described in terms of D and E using the standard spin-Hamiltonian for an $S = 1$ spin system (see the Experimental Section). We also made the crude assumption that the dipolar and g tensors were collinear.[35] Using this model, we could achieve only qualitative agreement between the simulated and experimental spectra. On the basis of these simulations, a zero-field splitting of roughly 0.2 cm^{-1} or less is consistent with the observed EPR spectra. Also, we note that the EPR spectrum of a monomeric triplet complex, [PhBP$_3$]Co(PMe$_3$), has been recorded and contains features qualitatively similar to those of **3.2** and **3.3** in the solid-state, including the low field g signal ~4.8. This system has been described elsewhere (see Chapter 5).[15c]
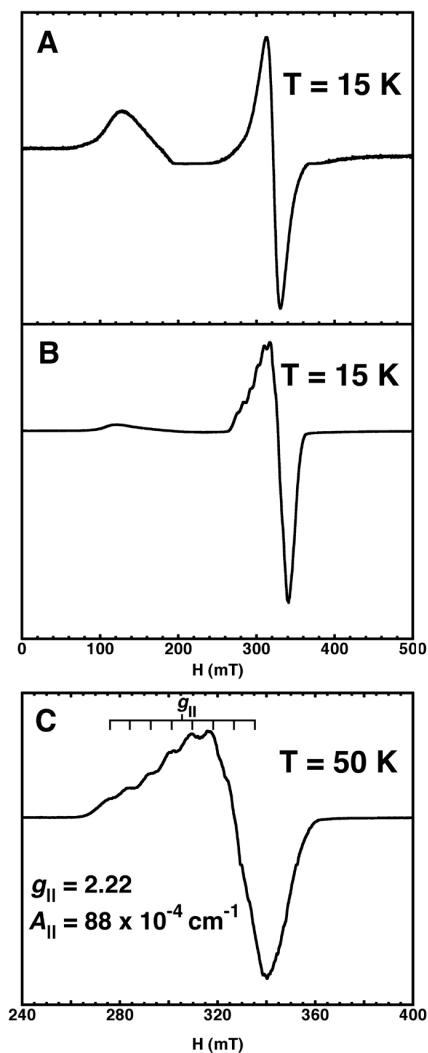
Figure 3.7. (A) EPR spectrum of a polycrystalline sample of ([PhBP$_3$]Co(μ-Br))$_2$ (**3.2**) at 15 K. (B) EPR spectrum of a glassy toluene solution of ([PhBP$_3$]Co(μ-Br))$_2$ at 12 K. (C) EPR spectrum of a glassy toluene solution of ([PhBP$_3$]Co(μ-Br))$_2$ at 50 K. $g_{||}$ and $A_{||}$ were estimated by simulating the EPR spectrum. See Experimental section for parameters.
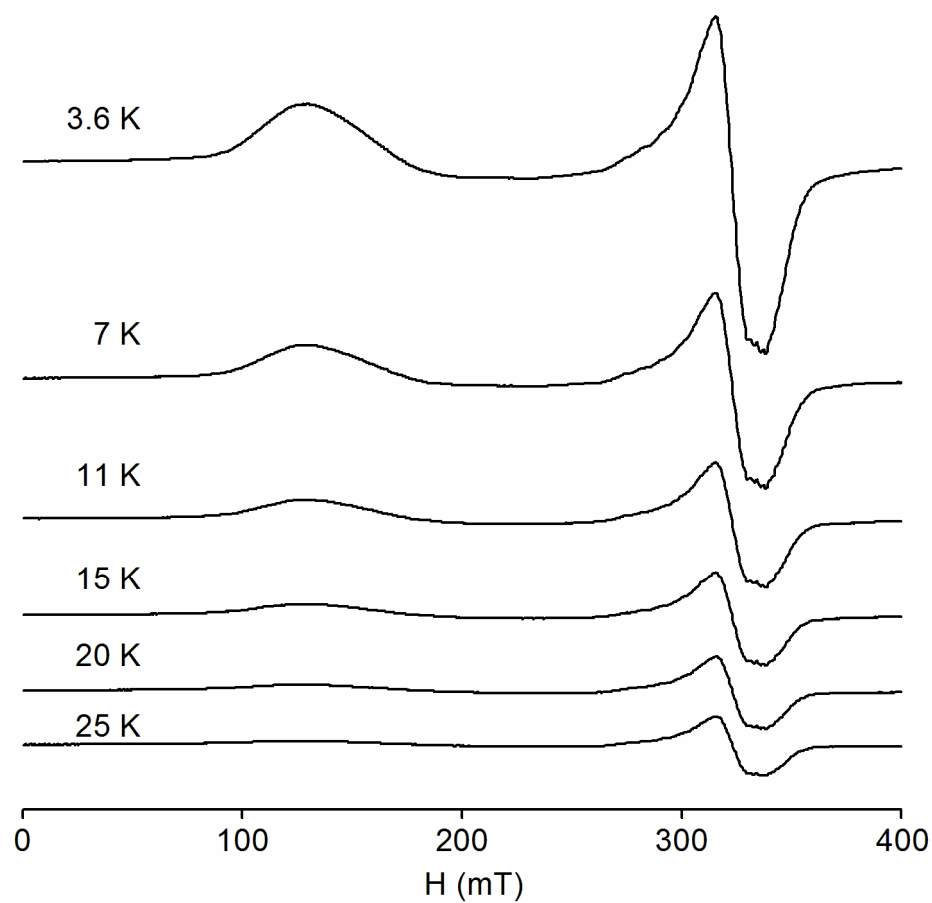
Figure 3.8. Series of EPR spectra for a polycrystalline sample of ([PhBP$_3$]Co(μ-Br))$_2$ (**3.2**) plotted to show the temperature dependence of the EPR signal. The signal amplitude increases as the temperature decreases, suggestive of a ferromagnetic triplet ground state.
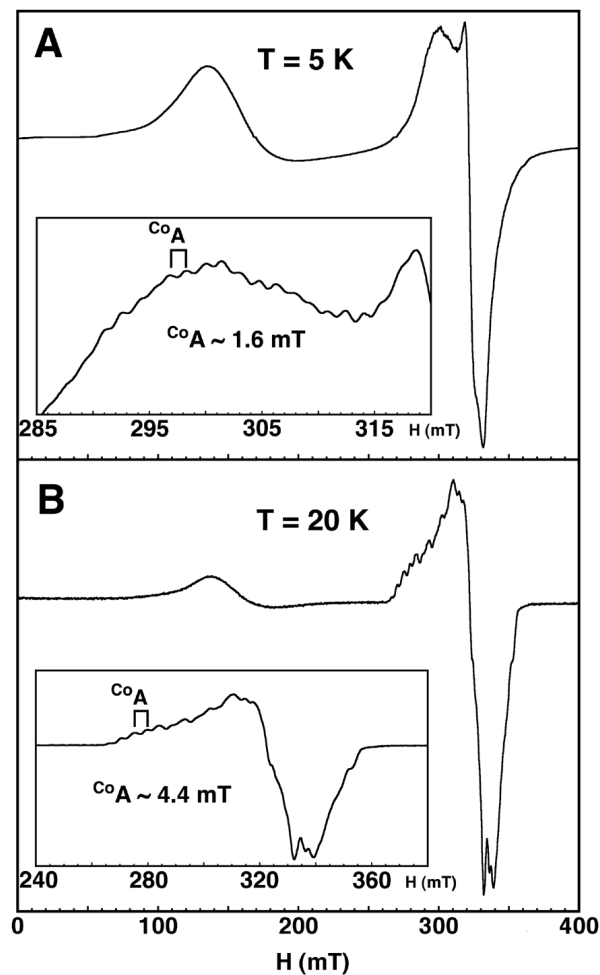
Figure 3.9. (A) EPR spectrum of a polycrystalline sample of ([PhBP$_3$]Co(μ-Cl))$_2$ (**3.3**) at 3.6 K. (B) EPR spectrum of a glassy toluene solution of ([PhBP$_3$]Co(μ-Cl))$_2$ at 12 K. See Experimental Section for parameters.

Dissolution of *purple* crystals of ([PhBP$_3$]Co(μ-Br))$_2$ (**3.2**) and ([PhBP$_3$]Co(μ-Cl))$_2$ (**3.3**) in toluene was accompanied by a drastic color change to bright green, similar to the color of [PhBP$_3$]CoI both in solution and in the crystalline state. This behavior suggested to us a structural change in the dimers **3.2** and **3.3** upon dissolution.

Indeed, we found by EPR that in solution a temperature-dependent equilibrium between monomeric and dimeric species seems to exist (Eq. 3.3). The EPR spectrum of **3.2** in glassy toluene (15 K) is shown in Figure 3.7. This spectrum presumably represents a monomeric species akin to the structurally characterized iodide monomer, perhaps with an additional trace presence of the dimeric form of **3.2**. The observation that $g_\parallel > g_\perp$ for **3.2** in the frozen glass clearly establishes that the square-pyramidal arrangement of the cobalt complex, observed in the solid-state, is not preserved in solution. We suggest that the geometry of **3.2** in solution is that of a pseudotetrahedral, 4-coordinate monomer, as for the case of **3.1**. The similarity of the magnetic moments for solutions of **3.1** and **3.2** is also consistent with their having similar coordination geometries. We therefore conclude that the glassy toluene EPR spectrum of **3.2** represents the monomeric and low spin complex [PhBP$_3$]CoBr. The resolved hyperfine coupling in the g$_\parallel$ region is in accord with this model ($A_\parallel = 88 \times 10^{-4}$ cm^{-1}) as it shows an octet, indicative of coupling to a single cobalt nucleus. If the dimer of **3.2** were maintained in solution, we would have expected to observe a 15-line splitting pattern. A related EPR study was also performed for the chloride **3.3**. The polycrystalline and glassy EPR spectra of **3.3**, shown in Figure 3.8 are similar to that of **3.2**. The major difference is that a readily detectable population of the dimer of **3.3** appears to be present in glassy toluene at 12 K. The low spin monomer [PhBP$_3$]CoCl, however, is the major species present in the glass even at this low temperature. The additional hyperfine resonances observed in the g$_\parallel$ region (~2.2) for **3.3** are also suggestive of a modest concentration of the triplet ([PhBP$_3$]Co(μ-Cl))$_2$ in the glassy toluene spectrum, which is superimposed with the signal expected for [PhBP$_3$]CoCl. The hyperfine coupling for [PhBP$_3$]CoCl is resolvable with $A_\parallel = 92 \times 10^{-4}$

cm^{-1}. The temperature dependence of the optical spectrum of **3.3** is discussed below and lends further support to the suggestion that **3.3** can dimerize in solution as a function of temperature.

$$(3.3)$$
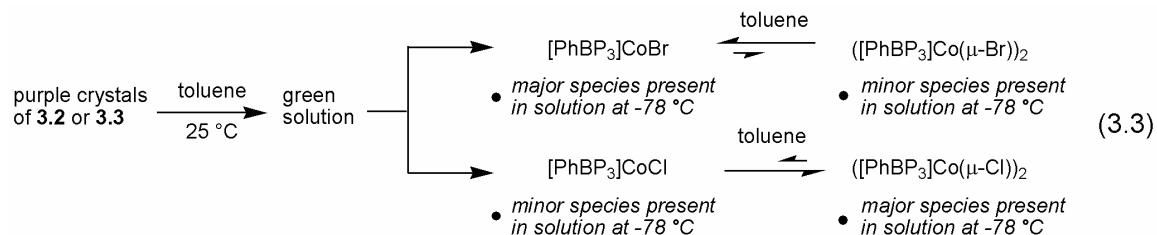
3.2.4 Conversion of low spin iodide to the high spin complex [PhBP₃]CoO(2,6-Me₂-C₆H₄)

It was prudent to prepare one or more complexes of similar geometry to **3.1** with a high spin ground state so that the relevant structural, magnetic, and spectroscopic data could be compared to the monomeric low spin derivatives already described.

$$(3.4)$$
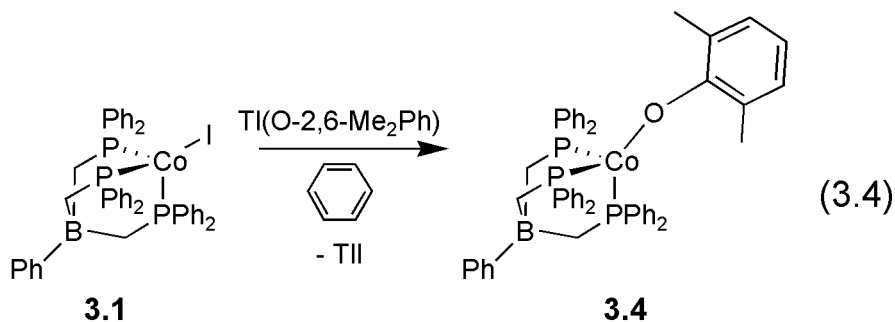
We prepared a more conventional four-coordinate and *high spin* complex supported by an intact [PhBP₃] ligand. The iodide complex **3.1** was allowed to react with the moderately bulky thallium aryloxide reagent Tl(O-2,6-Me₂-Ph), which smoothly generated the aryloxide species [PhBP₃]CoO(2,6-Me₂-Ph), (**3.4**), as a red-brown, crystalline solid (Eq. 3.4). The solid-state structure of **3.4**, depicted in Figure 3.10, reveals **3.4** to be monomeric, but grossly distorted from idealized threefold symmetry. Each of

the three O-Co-P angles is quite different (134.9(1)°, 120.4(1)°, and 105.3(1)°) and one

of the phosphine donor arms is slightly elongated by comparison to the other two

(2.366(1) Å versus 2.332(1) and 2.343(1) Å, respectively). High spin, four-coordinate

cobalt(II) systems typically adopt higher symmetry when possible; the distorted structure

obtained for **3.4** likely results from steric interactions between the bulky aryloxide and

[PhBP$_3$] ligands. The Co-P bond lengths in **3.4** are, on average, appreciably elongated in

comparison to **3.1** (~ 0.12 Å). This difference again qualitatively reflects their different
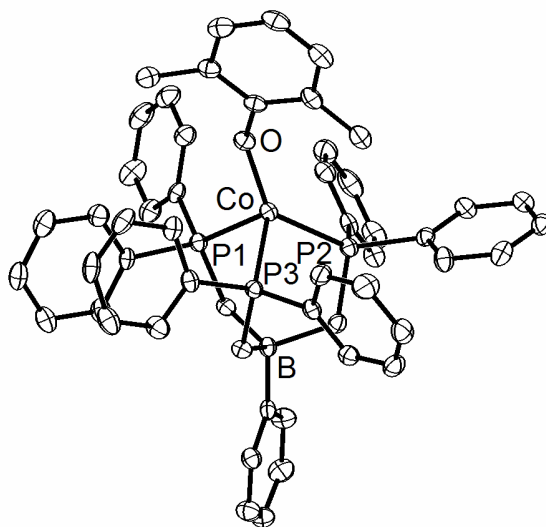
spin states.

Figure 3.10. Displacement ellipsoid representation (50%) of [PhBP$_3$]CoO(2,6-dimethylphenyl), (**3.4**). Selected interatomic distances (Å) and angles (deg): Co-O, 1.851(2); Co-P3, 2.332(1); Co-P2, 2.366(1); Co-P1, 2.343(1); Co-B, 3.446(3); O-Co-P3, 120.39(5); O-Co-P2, 134.93(5); P3-Co-P2, 98.27(2); O-Co-P1, 105.27(5); P3-Co-P1, 92.72(2); P2-Co-P1, 94.22(2).

3.2.5 Comparative magnetic and EPR characterization of [PhBP$_3$]CoO(2,6-Me$_2$-C$_6$H$_4$)

The aryloxide complex **3.4** also appears to be a high spin species in the solid-state, as evident from its SQUID data provided in Figure 3.4. Its high spin moment was maintained in solution (4.3 μ_B, C$_6$D$_6$, 25 °C). It is also interesting to note that the χ_mT versus T plot for **3.4** reveals an unexpected rise in χ_mT as the sample temperature is lowered. This rise becomes more dramatic at temperatures < 100 K and reaches a maximum at 16 K, at which point it falls precipitously to zero as the temperature is lowered further, perhaps suggestive of intermolecular antiferromagnetic exchange. The glassy toluene EPR spectrum of **3.4** also suggests that it is high spin and its signal is not detected at elevated temperatures (> 50 K).

3.2.6 Comparative optical spectra of [PhBP$_3$]CoI, ([PhBP$_3$]Co(μ-Br))$_2$, and ([PhBP$_3$]Co(μ-Cl))$_2$

The room temperature optical spectra for green solutions of **3.1**, **3.2**, and **3.3** (250-1500 nm) were obtained in toluene and are shown in Figure 3.11. The spectra for the halides **3.1**, **3.2**, and **3.3** are very similar and are dominated by an apparent broad charge-transfer band in the visible region that displays an expected blue shift from I⁻ (638 nm) to Br⁻ (612 nm) to Cl⁻ (594 nm). Lower energy features that show less halide dependence are also present in the spectrum of each of the three halides. It is important to note that incubation of green toluene solutions of **3.1** and **3.2** at -78 °C did not effect an appreciable color change. In contrast, incubation of a green solution of chloride **3.3** at -78 °C gave rise to a distinctly purple solution whose green color was recovered on warming. The inset spectrum shown in Figure 3.11 was acquired upon rapid removal of the purple

solution containing **3.3** from a -78 °C cold bath. In accord with the EPR data, we presume that this spectrum represents a superposition of the spectrum for the dimeric form of **3.3** and its monomeric, pseudotetrahedral low spin form. The optical spectrum of high spin **3.4** was also obtained in toluene solution. The visible region of its spectrum was characterized by broad features between 400 and 800 nm with resolvable maxima at 530, 580, and 752 nm.
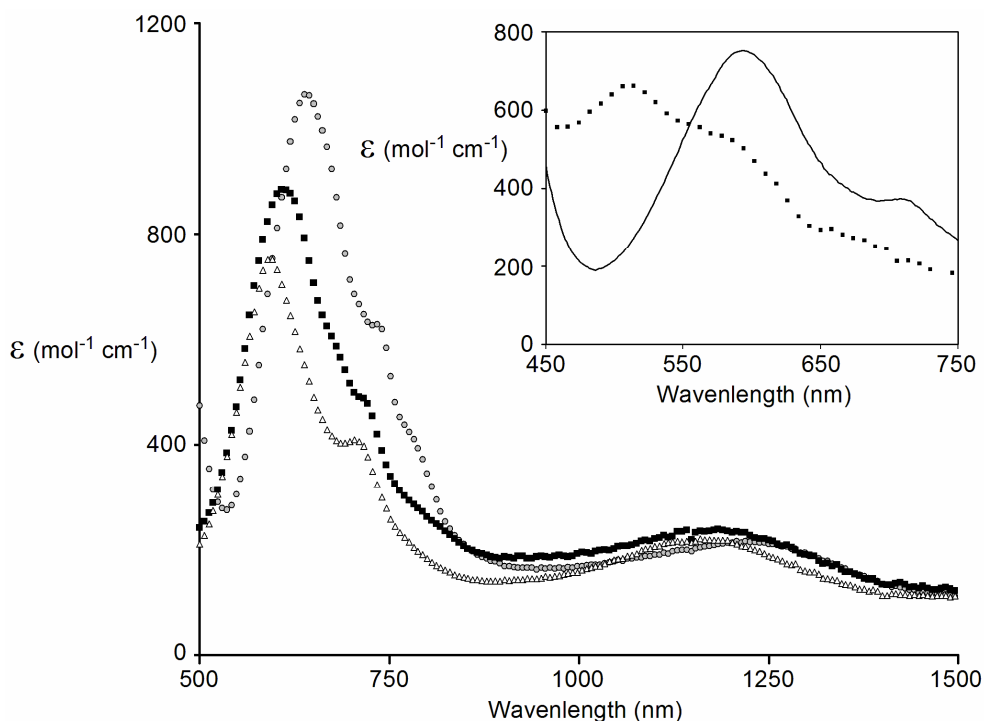
Figure 3.11. Absorption spectra for compounds $[PhBP_3]CoI$, **3.1**, (●), $([PhBP_3]Co(\mu\text{-Br}))_2$, **3.2**, (■), and $([PhBP_3]Co(\mu\text{-Cl}))_2$, **3.3**, (Δ), between 500 and 1500 nm. The similarity between each of the spectra suggests that each complex is predominantly monomeric at ambient temperature in toluene solution. **Inset:** $([PhBP_3]Co(\mu\text{-Cl}))_2$, **3.3**, at 298 K (——) and at 220 K (■) in toluene solution, illustrating the temperature dependence of the optical absorption that is associated with a monomer (298 K) to dimer (220 K) equilibrium.

3.3 Discussion

The preceding sections have presented structural, magnetic, and spectroscopic evidence to suggest that a low spin formulation is correct for *monomeric* [PhBP$_3$]CoX systems, where X represents the halides I$^-$, Br$^-$, or Cl$^-$. Although the iodide complex **3.1** is a simple four-coordinate monomer both in the solid-state and in solution, the chloride **3.3**, and to a lesser extent the bromide **3.2**, are capable of dimerizing to a modest degree in solution at low temperature; they both crystallize in the dimeric form. The solid-state SQUID and EPR data collected for the dimers **3.2** and **3.3** prompt us to assign them to triplet ground states exhibiting weak ferromagnetic coupling. A more detailed analysis of their electronic structures is worth pursuing in future studies, though it is at present clear that the electronic structures of **3.2** and **3.3** are quite distinct from the structurally related dimers of Sacconi, these latter systems being characterized by singlet ground states due to pronounced antiferromagnetic exchange.

At room temperature, both **3.2** and **3.3** are *predominantly monomeric* in solution.[36] Room temperature solutions of **3.1**, **3.2**, and **3.3** in toluene are bright green; solutions of **3.1** and **3.2** remain green on cooling to 195 K, whereas a solution of **3.3** turns purple (reversibly) as it is cooled, indicative of the dimer concentration at low temperature. The solution EPR spectra are also consistent with this model. At low temperatures (< 50 K), the EPR spectra of iodide **3.1** and bromide **3.2** show only the monomer form. For the chloride **3.3**, however, the dimeric form also appears to be present below 50 K, superimposed with the spectrum for the monomer. The optical spectra for the three complexes are in accord with these data. Each of the spectra shows

very similar features at room temperature, suggesting analogous stereochemical environments in solution. Cooling the solution of **3.3** causes a dramatic change in color from green to purple, reflecting the increase in concentration of its dimeric form.

The most intriguing observation concerns the low spin character of the monomeric form of these simple halide complexes. Configurational solution equilibria between high and low spin complexes of cobalt were first observed more than three decades ago.[5,37,38] The typical situation is as follows: a low spin pentacoordinate cobalt(II) complex can dissociate one ligand to afford (i) a high spin, tetrahedral or distorted tetrahedral structure type, or (ii) a low spin, square planar or distorted square planar structure type. In certain cases, a solution equilibrium has been observed between strictly four-coordinate structures that are high spin (tetrahedral) and low spin (square planar), such as the bis(β-ketoamino)cobalt(II) complexes described by Holm and Everett.[5a] Stereochemical tuning of a series of tropocoronand ligands coordinated to divalent cobalt by Lippard and co-workers was shown to give rise to a range of intermediate structure types that were classified as either distorted tetrahedral (and high spin) or distorted square planar (and low spin). The halides described in the present manuscript are anomalous in that, for complexes **3.2** and **3.3**, solution equilibria between a low spin, five-coordinate, distorted square pyramidal structure and a low spin, four-coordinate, distorted tetrahedral structure apparently exist. The X-ray crystal structure of the iodide complex **3.1** provides a structural snapshot of the distorted tetrahedral, low spin four-coordinate structure, a structure that is not directly observable for complexes **3.2** and **3.3**, but which is inferred from the solution data available for these complexes. It becomes apparent that a low spin state for four-coordinate cobalt(II) can be

achieved by a distortion strikingly different from the severe distortion that takes a tetrahedral structure to a square planar structure. In the present case, a more subtle distortion, one that is distinctly axial in character, gives rise to the low spin configuration. The following discussion, accompanied by Figures 3.12 and 3.13, provides a simple orbital explanation for this phenomenon.
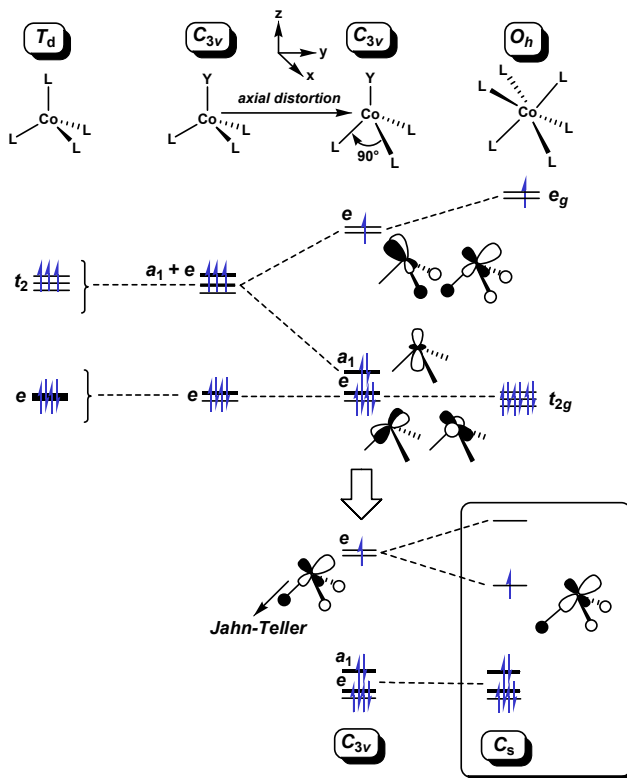
Figure 3.12. Qualitative d-orbital splitting diagram that depicts a descent in symmetry from T_d to C_{3v} symmetry for an axially distorted tetrahedral cobalt(II) system. As defined, the z-axis proceeds through one Co-L vector of the starting tetrahedron. The figure presents three limiting structure types: an idealized tetrahedron (CoL$_4$), a C_{3v} structure (CoYL$_3$) with bond angles analogous to the tetrahedral structure, and a C_{3v} structure resulting from a strong axial distortion (CoYP$_3$) in which the P-Co-P angle are fixed to ~90°.

A tetrahedral ligand-field for divalent cobalt places three degenerate orbitals, the t set, at a significantly higher energy than the nonbonding e set. Following Hund's rule, four electrons fill the e set, and three electrons fill the t set, one per orbital in a spin-aligned fashion. As is well-known, this is the origin of the typically observed quartet ground state that has been previously observed for tetrahedral and distorted tetrahedral cobalt(II) complexes. Breaking the symmetry, whether to C_3, C_s, or C_1, does not typically change this situation. The three orbitals at higher energy are only modestly split as the symmetry of the molecule descends from the tetrahedron. This splitting of the degenerate t set is typically small by comparison to the pairing energy that would be required to achieve a low spin state. However, if this splitting becomes large, and if an orbital of a_1 symmetry (predominantly dz^2) from the upper set is strongly stabilized on distortion, it should be possible to access a low spin population. We think that the stereochemical environment and the strong ligand-field donor-strength provided by the [PhBP$_3$] anion achieve this extreme and thereby provide access to the low spin ground state for pseudotetrahedral cobalt(II). The phosphine ligands of [PhBP$_3$] are good sigma-donors and should contribute to a strong ligand-field in pseudo-C_3 symmetry whereby the upper orbital set, σ^* in character, lies well above the lower nonbonding orbital set. The dominant factor to consider is the extent to which a hybrid a_1 orbital (predominantly dz^2 with some admixed s and p_z) is stabilized as the cobalt center is axially distorted along the Co-I vector (i.e., along z). When stabilization of this a_1 orbital becomes strong enough, and when the ligand-field is sufficiently strong so as to destabilize the now high-lying e-set, electron pairing becomes energetically favorable and a low spin ground state is achieved. Figure 3.12 summarizes this model schematically by correlating the low

spin configuration in idealized C_{3v} symmetry to idealized T_d and O_h structures. Note that the natural choice of coordinate axes for all of the structures shown in Figure 3.12 places the z-axis through one face of an octahedral ML_6. Although this definition of axes is obvious for C_{3v} symmetry, it is not the typical choice for O_h ML_6. To describe the orbital character of the lower t_{2g} and upper e_g sets, the orbital functions need to be correlated to the new coordinate axis system. For an O_h ML_6 complex, these functions transform as:[39]

t_{2g} set: z^2; $\{(2/3)^{1/2}(x^2 - y^2) - (1/3)^{1/2}yz\}$; $\{(2/3)^{1/2}xy - (1/3)^{1/2}xz\}$. **For e_g set:** $\{(1/3)^{1/2}x^2 - y^2 + (2/3)^{1/2}yz\}$; $\{(1/2)^{1/2}xy + (2/3)^{1/2}xz\}$. When the axial distortion is so severe that the angle (L-Co-L) between the three *fac* ligands becomes 90°, enforced in complex **3.1** by the [PhBP$_3$] ligand, the set of orbitals derived for O_h symmetry correlates very well with the axially distorted pseudotetrahedral structure type. For a low spin configuration we anticipate a Jahn-Teller distortion from C_{3v} to C_s symmetry. The lower portion of Figure 3.12 depicts this situation and suggests the final ground electronic configuration (using the functions given above) to be $(\{(2/3)^{1/2}(x^2 - y^2) - (1/3)^{1/2}yz\})^2(\{(2/3)^{1/2}xy - (1/3)^{1/2}xz\})^2(z^2)^2(\{(1/3)^{1/2}x^2 - y^2 + (2/3)^{1/2}yz\})^1(\{(1/2)^{1/2}xy + (2/3)^{1/2}xz\})^0$. The EPR spectrum of **3.1** ($g_{\parallel}$ = 2.20 and $g_{\perp}$ = 2.05) is consistent with this configuration to the extent that $g_{\parallel}$ is appreciably higher than the free electron value, suggesting that the unpaired spin is not localized in an orbital of dz^2 parentage. Rather, the unpaired spin resides in an orbital that is formally $\{(1/3)^{1/2}x^2 - y^2 + (2/3)^{1/2}yz\}$ within the present coordinate axis scheme.
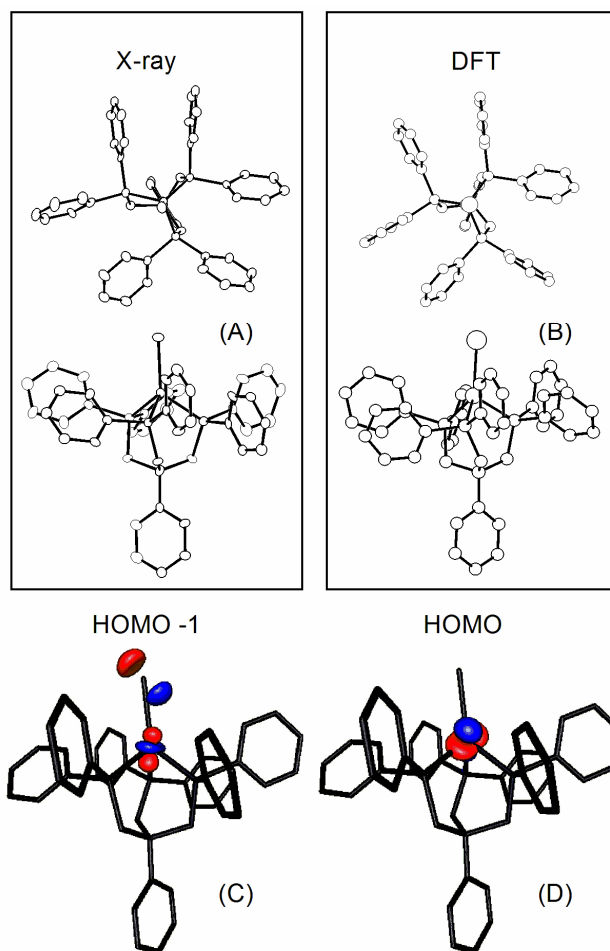
Figure 3.13. Figure shows the experimental (X-ray) **(A)** and calculated (DFT) **(B)** molecular structures for [PhBP$_3$]CoI (**3.1**). Representations of the HOMO-1 **(C)** and HOMO **(D)** orbitals obtained from the DFT electronic structure calculations are also shown. The calculated (DFT) bond distances (Å) and angles (deg) were theoretically determined to be as follows (the experimentally determined value is shown in parentheses): Co-I, 2.585 (2.474); Co-P(1), 2.282 (2.163); Co-P(2), 2.240 (2.208); Co-P(3), 2.402 (2.244); P(1)-Co-P(2), 88.6 (90.5); P(1)-Co-P(3), 96.0 (92.9); P(2)-Co-P(3), 90.5 (92.3); P(1)-Co-I, 119.0 (119.6); P(2)-Co-I, 131.6 (127.3); P(3)-Co-I, 121.6 (124.6).

Hoping to corroborate this conclusion, we performed a theoretical electronic structure calculation on the title complex **3.1**. The geometry of the complete complex, including the aryl rings of the [PhBP$_3$] ligand, was theoretically determined by performing a geometry optimization that used the experimentally determined structural coordinates for **3.1** as a starting point (see the Experimental Section for details). The structure calculation converged and reasonable, though not excellent, agreement between the theoretical structure of **3.1** and its experimentally determined structure was established (Figure 3.13). The electronic structure of **3.1** determined by DFT suggests the HOMO orbital to be one of π-antibonding character between the cobalt center and the iodide ligand, and the HOMO-1 orbital to be predominantly dz^2 in character, in accord with the qualitative MO scheme presented in Figure 3.12.

Although a great many high spin distorted tetrahedral complexes are known, two systems that deserve to be singled out with respect to the present discussion are the monomeric halides [Tp'']CoI ([Tp''] = hydrotris(3-*tert*-butyl-5-methylpyrazolyl)borate) and [Tt$^{tert\text{-butyl}}$]CoCl ([Tt$^{tert\text{-butyl}}$] = [PhB(CH$_2$S^{t}Bu)$_3$]$^-$), each of which has been structurally characterized and assigned as high spin.[22,23] Like complex **3.1**, they each have approximate C_3 symmetry, and like complex **3.1**, they have a borate atom placed in close proximity to the cobalt center along the *z*-axis. The X-ray structures of [Tp'']CoI and [Tt$^{tert\text{-butyl}}$]CoX also show a rather strong distortion in the axial direction (the average I-Co-N angle is ~122° for [Tp'']CoI; the average Cl-Co-S angle is ~118° for [Tt$^{tert\text{-butyl}}$]CoCl). Geometric constraints for the facially capping [PhBP$_3$], [Tp''] and [Tt$^{tert\text{-butyl}}$] donor ligands enforce the large X-Co-L (L = P, N, and S donor, respectively) bond angles in each case. As previously mentioned, low spin **3.1** is somewhat distorted

from C_3 symmetry by elongation of one of the phosphine donors. A similar distortion is not observed in [Tp'']CoI or [Tt$^{tert\text{-}butyl}$]CoCl. In these three cases, the three Co-L (L = N, S) bond lengths are very similar and the three X-Co-L bond angles show little variation. The solid-state structure of **3.1** is a reasonable consequence of its low spin configuration, expected to give rise to a Jahn-Teller distortion. That the related complexes [Tp'']CoI and [Tt$^{tert\text{-}butyl}$]CoCl do not adopt a low spin configuration and show a similar Jahn-Teller distortion likely reflects the relative ligand-field donor strengths of the three borate-derived donor ligands. The upper lying e-set (in C_{3v}) is σ*. Its degree of destabilization should directly reflect the relative donor strength of three donor ligands. The [PhBP$_3$] ligand appears to be the strongest donor, destabilizing the upper orbital set to the greatest extent, but by a relative amount that has yet to be quantified. The ability of each ligand to accommodate a Jahn-Teller distortion (if a low spin configuration is to occur), however, is also a variable that needs to be considered. Tris(pyrazolyl)borate ligands, when coordinated in an η^3-fashion, are not very flexible. Geometric Jahn-Teller distortion to a stable low spin configuration might therefore be energetically unfavorable. Thus, [Tp]-derived ligands could provide a ligand-field strength similar to [PhBP$_3$], but still be coordinatively less flexible, thereby raising the energy of the doublet state above the quartet state for [Tp]CoX derivatives. Riordan's [Tt$^{tert\text{-}butyl}$]CoCl complex is another matter. That the monomeric complex [Tt$^{tert\text{-}butyl}$]CoCl is high spin is somewhat surprising based on the electronic scheme presented herein. It would seem that the tris(thioether)borate ligands are flexible enough to permit the Jahn-Teller distortion. The high-spin character of [Tt$^{tert\text{-}butyl}$]CoCl is perhaps reflective of their less pronounced axial elongation and an attenuated ligand-field strength by comparison to the [PhBP$_3$]CoX

systems. This would have the effect of narrowing the gap between the a_1 orbital and the upper e manifold, thereby making the high spin configuration of [Tt$^{tert\text{-}butyl}$]CoCl more stable. It would certainly be of interest to comparatively study the temperature dependence of the magnetic behavior of Theopold's and Riordan's cobalt(II) systems by SQUID magnetometry to establish whether any of the low spin forms for these complexes is populated at very low temperatures.

An interesting observation for the low spin complexes **3.1**, **3.2**, and **3.3** is that they bind a stoichiometric equivalent of CO readily to form the low spin, 5-coordinate carbonyl adducts [PhBP$_3$]Co(CO)(X) (X = I$^-$, Br$^-$, Cl$^-$). It is of interest in the present discussion to compare the relative CO donor strength of [PhBP$_3$]Co(CO)(Br) to the isostructural but cationic complex [(H$_3$CC(CH$_2$PPh$_2$)$_3$)Co(Br)(CO)][BPh$_4$] previously reported by Sacconi.[19d] The carbonyl stretching frequency of [PhBP$_3$]Co(CO)(Br) is 2030 cm^{-1}. The carbonyl stretching frequency of structurally characterized [(H$_3$CC(CH$_2$PPh$_2$)$_3$)Co(Br)(CO)][BPh$_4$] is 2060 cm^{-1}. That the cationic complex exhibits a CO stretch 30 cm^{-1} higher in energy than the neutral derivative suggests that the anionic borato ligand is an appreciably stronger donor than its neutral ligand counterpart. The increased donor strength likely accounts for the tendency of dimeric bromide **3.2** to dissociate to a 15 electron, low spin monomer in solution. Such an equilibrium has not been observed for any of the cationic cobalt(II) dimers supported by triphos, in which a halide or pseudohalide occupies the bridging position.[19,20] We highlight this distinction because it is important to bear in mind with respect to the degree of "zwitterionic" character ascribed to neutral complexes supported by (phosphino)borate ligands. From the perspective of a simple Lewis structure depiction, simple resonance contributors that

delocalize the anionic borate charge to the phosphine donor ligands are not available. This contrasts the situation for tris(pyrazolyl)borate ligands, where simple resonance delocalization is expected to partially distribute the negative charge to the N-donor atoms. That [PhBP$_3$] is such a strong field donor, however, suggests that there is appreciable communication between the borate anion and the bound metal center, either through space or through the sigma framework. Our ability to identify low spin, monomeric cobalt(II) halides that do not irreversibly dimerize might be a direct consequence of the strong field of the [PhBP$_3$] anion: it stabilizes complexes that are formally electron deficient. The high spin complex **3.4** is also monomeric, as are the high spin systems of Theopold and Riordan.[22,23] This is perhaps to be anticipated, as they do not possess an empty *d* orbital to accommodate the lone pair of a bridging halide ligand. In accord with this model, we note that the high spin cobalt(II) derivative **3.4**, in addition to the Riordan and Theopold systems, appears to be more resistant to coordination of carbon monoxide. This fact may, however, simply reflect other factors such as relative ligand-field donor strengths and steric considerations.

3.4 Conclusion

In summary, we have synthesized and studied a series of divalent cobalt complexes supported by [PhBP$_3$]. Structural, magnetic, and spectroscopic data for each of these systems is suggestive of low spin behavior for their monomeric, distorted tetrahedral structure types. The low spin nature of the monomeric form of these halides appears to be unique from related systems that have been previously studied. Two scenarios that transform a high spin, 4-coordinate tetrahedral complex to a four-coordinate species that is low spin can therefore be put forward. The first scenario

pertains to the traditional case in which a high spin tetrahedral structure is distorted to a low-spin square planar structure type. The second scenario, that which is described herein, occurs when coupling of a strong ligand-field donor strength with a pronounced axial distortion leads to a distorted tetrahedral geometry that can accommodate a cobalt(II) ion in a low spin ground-state configuration. The latter, more gentle distortion exposes an orbital at the cobalt(II) center appropriate for small molecule binding, a feature that could be exploited if tunable crossover systems for four-coordinate cobalt(II) prove accessible. We are pursuing this possibility by searching for new $[PhBP_3]CoX$ systems that display spin crossover phenomena while maintaining four-coordination in an approximate tetrahedral structure type. We are also pursuing new tris(phosphino)borate ligands to further test our electronic model.

3.5 Experimental section

3.5.1 General considerations

General procedures were performed according to Section 2.4.1. Three additional instruments were employed. UV-vis measurements were taken on a Hewlett-Packard 8452A diode array spectrometer using a quartz crystal cell with a Teflon cap. Near-IR measurements were taken on a Cary 14 spectrophotometer using a quartz crystal cell with a Teflon cap. IR measurements were obtained using a Bio Rad Excalibur FTS 3000 with a KBr solution cell. The ^{1}H NMR assignments for **3.1** were determined by a combination of T_1 relaxation rates and single scan integrations.

3.5.2 Magnetic measurements

Measurements were recorded using a Quantum Designs SQUID magnetometer running MPMSR2 software (Magnetic Property Measurement System Revision 2). Data

were recorded at 5000 G. Samples were suspended in the magnetometer in plastic straws

sealed under nitrogen with Lilly No. 4 gel caps. Each measurement was performed on

samples that had been recently subjected to combustion analysis to verify their purity.

Loaded samples were centered within the magnetometer using the DC centering scan at

35 K and 5000 gauss. Data were acquired at 2-10 K (one data point every 2 K), 10-60 K

(one data point every 5 K), 60-310 K (one data point every 10 K).

The magnetic susceptibility was adjusted for diamagnetic contributions using the

constitutive corrections of Pascal's constants. The molar magnetic susceptibility (χ_m) was

calculated by converting the calculated magnetic susceptibility (χ) obtained from the

magnetometer to a molar susceptibility (using the multiplication factor {(molecular

weight)/[(sample weight)(Field Strength)]}). Curie-Weiss behavior was verified by a plot

of χ_m^{-1} versus T. Data were analyzed using Eqs. 3.5 and 3.6. Average magnetic moments

were taken from the average of magnetic moments from the ranges indicated in the

Experimental Section for each complex. The Weiss constant (θ) was taken as the

x-intercept of the plot of χ_m^{-1} versus T. Error bars were established at 95% confidence

using regression analysis or taking two standard deviations from the mean. Solution

magnetic moments were measured by the method of Evans and were adjusted for

diamagnetic contributions using the constitutive corrections of Pascal's constants.

$$\chi_m = \frac{\chi M}{mG} \quad (3.5) \qquad \mu_{eff} = \sqrt{7.997\chi_m T} \quad (3.6)$$

Averaged g-factors can be extracted from the susceptibility data, assuming zero

orbital contributions, using the following equation:

$$\chi_m = \frac{Ng^2\beta^2}{3kT}(S(S+1)) \quad (3.7)$$

3.5.3 EPR measurements

X-band EPR spectra were obtained on a Bruker EMX spectrometer equipped with a rectangular cavity working in the TE_{102} mode. Variable temperature measurements were conducted with an Oxford continuous-flow helium cryostat (temperature range 3.6-300 K). Accurate frequency values were provided by a frequency counter built in the microwave bridge. Solution spectra were acquired in toluene for all of the complexes. Sample preparation was performed under a nitrogen atmosphere, *particularly* important for handling the low spin complexes **3.1**, **3.2**, and **3.3**.

EPR simulations for the monomers were performed with the program WINEPR *SimFonia* (Version 1.25, Bruker Analytische Messtechnik GmbH); this software is based on second-order perturbation solution of the spin Hamiltonian: $H = H \cdot g \cdot S + \Sigma S \cdot A \cdot I$. For the dimers, the absolute values of the spin-Hamiltonian parameters were extracted from simulations of the EPR spectra. Calculations were carried out on a PC using FORTRAN code based on Gladney's general EPR fitting program[40] and adapted for simulations of EPR spectra of randomly oriented spin triplets. Transition fields and corresponding average transition moments[41] were computed in the magnetic field domain by matrix diagonalization of the $S = 1$ spin Hamiltonian.

$$\hat{H} = \beta(g_z H_z S_z + g_x H_x S_x + g_y H_y S_y) + D(S_z^2 - \tfrac{3}{2}) + E(S_x^2 - S_y^2) \quad (3.8)$$

D and E are defined in terms of the components of the diagonal fine-structure tensor as follows:

$$D_{zz} = 2D/3; \quad D_{xx} = -D/3; \quad D_{yy} = (-D/3) - E \quad (3.9)$$

Instrumental parameters for the spectra shown are as follows:

For [PhBP$_3$]CoI (**3.1**) in Figure 3.6: (A) EPR spectrum of a glassy toluene solution of [PhBP$_3$]CoI at 17 K. Instrumental parameters: ν = 9.477 GHz, modulation frequency = 100 kHz, modulation amplitude = 4 G, microwave power = 0.51 mW, conversion time = 81.92 ms, time constant = 20.48 ms, 3 scans. $g \approx 2$ region and spectral assignment; $g_\parallel$ and $A_\parallel$ were estimated by simulating the EPR spectrum (inset). (B) EPR spectrum of a glassy toluene solution of [PhBP$_3$]CoI in toluene-d_8 at 15 K. Instrumental parameters: ν = 9.476 GHz, modulation frequency = 100 kHz, modulation amplitude = 3 G, microwave power = 0.202 mW, conversion time = 81.92 ms, time constant = 20.48 ms, sweep time = 83.9 s, 3 scans.

For ([PhBP$_3$]Co(μ-Br))$_2$ (**3.2**) in Figure 3.7: (A) EPR spectrum of a polycrystalline sample of ([PhBP$_3$]Co(μ-Br))$_2$ (15 K). Instrumental parameters: ν = 9.480 GHz, modulation frequency = 100 kHz, modulation amplitude = 4 G, microwave power = 1.01 mW, conversion time = 163.84 ms, time constant = 40.96 ms, 10 scans. (B) EPR spectrum of a glassy toluene solution of ([PhBP$_3$]Co(μ-Br))$_2$ at 12 K. Instrumental parameters: ν = 9.472 GHz, modulation frequency = 100 kHz, modulation amplitude = 4 G, microwave power = 0.101 mW, 1 scan. (C) EPR spectrum of a glassy toluene solution of ([PhBP$_3$]Co(μ-Br))$_2$ at 50 K. $g_\parallel$ and $A_\parallel$ were estimated by simulating the EPR spectrum. Instrumental parameters: ν = 9.477 GHz, modulation frequency = 100 kHz, modulation amplitude = 5 G, microwave power = 2.02 mW, conversion time = 20.48 ms, time constant = 5.12 ms, 20 scans. (D) Series of EPR spectra for a polycrystalline sample of ([PhBP$_3$]Co(μ-Br))$_2$ plotted to show the temperature dependence of the EPR signal.

The signal amplitude increases as the temperature decreases, suggestive of a ferromagnetic triplet ground state.

For ([PhBP$_3$]Co(μ-Cl))$_2$ (**3.3**) in Figure 3.9: (A) EPR spectrum of a polycrystalline sample of ([PhBP$_3$]Co(μ-Cl))$_2$ at 3.6 K. Instrumental parameters: ν = 9.477 GHz, modulation frequency = 100 kHz, modulation amplitude = 4 G, microwave power = 0.101 mW, conversion time = 163.84 ms, time constant = 40.96 ms, 4 scans. (B) EPR spectrum of a glassy toluene solution of ([PhBP$_3$]Co(μ-Cl))$_2$ at 12 K. Instrumental parameters: ν = 9.476 GHz, modulation frequency = 100 kHz, modulation amplitude = 4 G, microwave power = 0.202 mW, conversion time = 163.84 ms, time constant = 40.96 ms, 7 scans. The inset $g \approx 2$ region showing resolved cobalt hyperfine structure; $g_{\parallel}$ and $A_{\parallel}$ were estimated by simulating the EPR spectrum.

3.5.4 DFT calculations

A geometry optimization was performed for complex **3.1** using Jaguar (Version 4.1) starting from coordinates based on the solid-state structure that had been determined by X-ray diffraction. No symmetry constraints were imposed, and the calculation was performed on a doublet electronic state. The method used was B3LYP with LACVP** as the basis set (modified to LACVP**++ for the boron atom). Optimization was considered converged when energy changes in successive iterations fell below 0.3 kcal/mol. It should also be noted that convergence was also achieved for a system when the geometry was optimized assuming a quartet ground state.

3.5.5 Starting materials and reagents

The preparation of [PhBP$_3$]Tl has been previously reported. TlO-2,6-Me$_2$Ph was prepared according to a literature procedure.[42] The reagents CoI$_2$, CoBr$_2$, CoCl$_2$, CO, O$_2$,

KBr, NaCl, and TlPF$_6$ were purchased from commercial vendors and used without further

purification.

3.5.6 Synthesis of compounds

Synthesis of [PhBP$_3$]CoI, 3.1. A benzene solution (50 mL) of the thallium reagent,

[PhBP$_3$]Tl, (0.356 g, 0.400 mmol) was added to a stirring suspension of CoI$_2$ (0.250 g,

0.799 mmol) in benzene (20 mL). After stirring at ambient temperature for 24 h, the

resulting green solution was filtered through diatomaceous earth, concentrated in vacuo

(50% original volume), and filtered through diatomaceous earth once again. Vapor

diffusion of petroleum ether into the resulting green filtrate afforded the pure crystalline

product (0.317 g, 91.1%), which was analyzed: ^{1}H NMR (C$_6$D$_6$, 300 MHz): δ 22.3 (6 H,

T$_1$ = 2.4 ms, PhB(CH_2PPh$_2$)$_3$), 10.8 (12 H, T$_1$ = 23.6 ms, *meta* P(C$_6$$H_5$)$_2$), 7.7 (2 H, T$_1$ =

40.5 ms, *ortho* B(C$_6$$H_5$)), 7.5 (3 H, T$_1$ = 205 ms, *meta* and *para* B(C$_6$$H_5$)), 4.3 (12 H, T$_1$ =

1.2 ms, *ortho* P(C$_6$$H_5$)$_2$), 2.2 (6 H, T$_1$ = 46.7 ms, *para* P(C$_6$$H_5$)$_2$). IR (cm^{-1}): 1433, 1091,

739. UV-vis (C$_6$H$_6$) λ$_{max}$, nm (ε): 638 (1112), 738 (627). SQUID (solid - average

30-220K): χ$_m$T = 0.88 cm^3 K mol^{-1}, θ = -1.43 K. Evans Method (C$_6$D$_6$): 2.76 μ$_B$. Anal.

Calcd for C$_{45}$H$_{41}$BCoIP$_3$: C, 62.03; H, 4.74. Found: C, 61.76; H, 4.75.

Synthesis of ([PhBP$_3$]Co(μ-Br))$_2$, 3.2. A benzene solution (50 mL) of the thallium

reagent, [PhBP$_3$]Tl (0.507 g, 0.570 mmol), was added to a stirring suspension of CoBr$_2$

(0.250 g, 1.14 mmol) in benzene (20 mL). After stirring at ambient temperature for 24 h,

the resulting green solution was filtered through diatomaceous earth. The filtrate was

pumped to dryness to leave a purple powder that was redissolved in benzene (20 mL),

filtered over diatomaceous earth, and again thoroughly dried in vacuo. A UV-vis

spectrum of this powder suggested a mixture of products. The powder was redissolved in

benzene (5 mL) and filtered over a fine sintered-glass frit. A microcrystalline purple powder precipitated from the solution; this powder (0.132 g, 28.1%) was dried and analyzed: ^{1}H NMR (C$_6$D$_6$, 300 MHz): δ 26.7, 11.0, 7.6, 7.4, 4.2, 2.2. UV-vis (C$_6$H$_6$) λ_{max}, nm (ε): 612 (1773), 718 (958). SQUID (solid, average 10-100 K): χ_mT = 0.39 cm^3 K mol^{-1}, θ = -1.48 ± 0.49 K; (solid, average 110-310 K) χ_mT = 0.56 cm^3 K mol^{-1}. Evans Method (C$_6$D$_6$, calculated for a monomer): 2.6 μ_B. Anal. Calcd for C$_{90}$H$_{82}$B$_2$Br$_2$Co$_2$P$_6$: C, 65.56; H, 5.01. Found: C, 65.23; H, 4.87. The sample used for the EPR and SQUID measurements, which was recrystallized two more times, analyzed as follows: C, 65.70; H, 5.04.

Synthesis of ([PhBP$_3$]Co(μ-Cl))$_2$, 3.3. A benzene solution (50 mL) of the thallium reagent, [PhBP$_3$]Tl (0.857 g, 0.963 mmol), was added to a stirring suspension of CoCl$_2$ (0.250 g, 1.93 mmol) in benzene (20 mL). After stirring at ambient temperature for 24 h, the resulting green solution was filtered through diatomaceous earth. The filtrate was dried in vacuo to a purple powder that was then redissolved in benzene (20 mL), filtered over diatomaceous earth, and again thoroughly dried. The resulting purple powder was redissolved in benzene (5 mL) and filtered over a fine sintered-glass frit; this caused a microcrystalline purple powder to precipitate from solution. The dried powder (0.195 g, 25.9%) was analyzed: ^{1}H NMR (C$_6$D$_6$, 300 MHz): δ 31.9, 11.2, 7.7, 7.4, 3.9, 2.2. UV-vis (C$_6$H$_6$) λ_{max}, nm (ε): 594 (1507), 712 (724). SQUID (solid - average 10-100 K): χ_mT = 0.76 cm^3 K mol^{-1}, θ = -3.13 ± 0.67 K; (solid - average 110-310 K) χ_mT = 0.97 cm^3 K mol^{-1}. Evans Method (C$_6$D$_6$, calculated for a monomer): 2.8 μ_B. Anal. Calcd for C$_{90}$H$_{82}$B$_2$Cl$_2$Co$_2$P$_6$: C, 69.30; H, 5.30. Found: C, 68.14; H, 5.18. The sample used for the

EPR and SQUID measurements, which was recrystallized two more times, analyzed as follows: C, 69.56; H, 5.36.

Alternative Preparation for 3.2 and 3.3. Thallium hexafluorophosphate (0.090 g, 0.26 mmol) was added to a stirring THF (20 mL) solution of **3.1** (0.201 g, 0.231 mmol). A yellow powder precipitated within 5 min and was subsequently removed by filtration through diatomaceous earth. NaCl (0.26 g, 4.4 mmol) was added to the filtrate, and the reaction solution was allowed to stir for 24 h. The above process was then repeated with additional $TlPF_6$ and NaCl. After another 24 h, the salts were removed by filtration; a UV-vis spectrum of the product solution indicated that **3.1** had been fully consumed, and the spectrum matched that of **3.3**. The solution was concentrated in vacuo to 50% of its original volume and allowed to stand for 24 h. White precipitate (NaCl) was removed by filtration, and the green solution was concentrated to dryness, redissolved in benzene, and once again allowed to stand for 12 h. Repeated filtration through diatomaceous earth ensured complete removal of salts. The final product was obtained by drying thoroughly in vacuo to afford purple **3.3** as a fine powder (0.159 g, 88.6%). An analogous protocol was effective for converting **3.1** to **3.2**, in this case using KBr instead of NaCl. Both UV-vis and ^1H NMR spectroscopies are useful in monitoring the metathesis procedure to ensure complete conversion.

Synthesis of [PhBP$_3$]CoO(2,6-dimethylphenyl), 3.4. A THF solution (5 mL) of the thallium reagent Tl-O-2,6-dimethylphenyl (0.0433 g, 0.133 mmol) was added to a stirring solution (10 mL) of **3.1** (0.116 g, 0.133 mmol). A yellow precipitate (TlI) formed within 15 min and was removed by filtration through diatomaceous earth. The remaining brown solution was stirred overnight. The reaction volatiles were removed in vacuo and the

resulting brown powder was redissolved in benzene. The benzene was lyophilized to thoroughly remove any remaining THF. The resulting fine powder was filtered once more through diatomaceous earth as a benzene (3 mL) solution. Vapor diffusion of petroleum ether into this benzene solution afforded the red-brown, crystalline product (0.067 g, 58.7% yield) that was analyzed. ^{1}H NMR (C_6D_6, 300 MHz): δ 67.0, 52.4, 17.9, 12.4, 11.6, 11.0, 9.0, 8.45, 7.80, 7.45, 7.06, -3.4, -6.5, -62.2. UV-vis (C_6H_6) λ_{max}, nm: 534 (1740), 752 (624). SQUID (solid, average 30-310 K): $\chi_mT = 2.41$ cm^3 K mol^{-1}, θ = 7.48 K. Evans Method (C_6D_6): 4.4 μ_B. Anal. Calcd for $C_{53}H_{50}BCoP_3O$: C, 73.54; H, 5.82. Found: C, 73.32; H, 5.95.

Synthesis of [PhB(CH$_2$P(O)Ph$_2$)$_2$(CH$_2$PPh$_2$)]CoI, 3.5. A 100 mL Schlenk flask with a Teflon stir bar was charged with a benzene (30 mL) solution of **3.1** (0.278 g, 0.319 mmol) and stirred at room temperature. Oxygen (7.8 mL at 1 atm, 0.32 mmol) was added to the reaction vessel via syringe through a rubber septum. After 4 h, the solution, which had turned bright blue, was dried in vacuo to a fine blue powder. Washing this powder with petroleum ether (3 x 10 mL) and concentrating it to dryness afforded the final product (0.225 g, 79.1% yield) that was analyzed. ^{1}H NMR (C_6D_6, 300 MHz): δ 16.2, 13.8, 10.1, 9.47, 9.28, 7.90, 7.09, -2.1. UV-vis (C_6H_6) λ_{max}, nm (ε): 590 (450), 642 (461), 682 (520). IR (cm^{-1}): 1435, 1126, 1095, 1071, 752. SQUID (solid, average 30-310 K): $\chi_mT = 2.34$ cm^3 K mol^{-1}, θ = -2.74 K. Evans Method (C_6D_6): 4.4 μ_B. Anal. Calcd for $C_{45}H_{41}BCoIP_3O_2$: C, 59.83; H, 4.57. Found: C, 59.62; H, 4.80.

Synthesis of [PhBP$_3$]Co(Br)(CO), 3.6. A 100 mL Schlenk flask with a Teflon stir bar was charged with a benzene (30 mL) solution of **3.2** (0.107 g, 0.0649 mmol) and stirred at room temperature until completely dissolved. Carbon monoxide (3.2 mL at 1 atm,

0.13 mmol) was added via syringe. After 4 h, the solution was frozen and the benzene was lyophilized, leaving a fine green powder. Washing this powder with petroleum ether (3 x 10 mL) and concentrating it to dryness afforded pure product (0.099 g, 89% yield). ^{1}H NMR (C_6D_6, 300 MHz): δ 13.8, 10.2, 8.1, 7.9, 7.5, 6.0. UV-vis (THF) λ_{max}, nm (ϵ): 676 (870). IR (THF, KBr solution cell, cm^{-1}): 2030. SQUID (solid – average 10 – 310 K): $\chi_m T = 0.50$ cm^3 K mol^{-1}. EPR (THF, 100 K): $g_\parallel = 2.30$, $A_{\parallel(Co)} = 33$ gauss, $A_{\parallel(P)} = 35$ gauss, $g_\perp = 2.05$, $A_{\perp(Co)} = 17$ gauss, $A_{\perp(P)} = 35$ gauss. Anal. Calcd for $C_{46}H_{41}BBrCoP_3O$: C, 64.82; H, 4.85. Found: C, 65.03; H, 5.59.

3.5.7 X-ray experimental information

The general X-ray experimental procedure was performed according to section 2.4.4. Crystallographic information is provided in Table 3.1.

Table 3.1. X-ray diffraction experimental details for [PhBP$_3$]CoI (**3.1**), ([PhBP$_3$]Co(μ-Br))$_2$ (**3.2**), ([PhBP$_3$]Co(μ-Cl))$_2$ (**3.3**), and [PhBP$_3$]CoO(2,6-Me$_2$-Ph) (**3.4**).

	[PhBP$_3$]CoI, (**3.1**)	([PhBP$_3$]Co(μ-Br))$_2$ (**3.2**)
Chemical formula	C$_{45}$H$_{41}$BCoIP$_3$ · ½ C$_6$H$_6$	C$_{90}$H$_{82}$B$_2$Br$_2$Co$_2$P$_6$
Formula weight	910.38	1648.68
T (ºC)	-177	-177
λ (Å)	0.71073	0.71073
a (Å)	22.5443(17)	22.214(3)
b (Å)	12.7044(9)	19.286(3)
c (Å)	29.526(2)	18.008(3)
α (º)	90	90
β (º)	90.230(2)	90
γ (º)	90	90
V (Å^3)	8456.6(11)	7715.0(19)
Space group	*P*2$_1$/c	*Pbcn*
Z	8	4
Dcalcd (g/cm^3)	1.430	1.419
μ(cm^{-1})	12.74	16.37
R1, wR2 (I>2σ(I))^a	0.0899, 0.0843	0.1432, 0.1012

[a] $R1 = \Sigma \, | \, |F_o| - |F_c| \, | \, / \, \Sigma \, |F_o|$, $wR2 = \{ \, \Sigma \, [\, w(F_o^2 - F_c^2)^2 \,] \, / \, \Sigma \, [\, w(F_o^2)^2 \,] \, \}^{1/2}$

Table 3.1. (cont.)

	([PhBP₃]Co(μ-Cl))₂ (**3.3**)	[PhBP₃]CoO(2,6-Me₂-Ph) (**3.4**)
Chemical formula	$C_{90}H_{82}B_2Co_2Cl_2P_6 \cdot 2\ C_6H_6$	$C_{53}H_{50}BCoOP_3$
Formula weight	1715.97	865.58
T (°C)	-177	-177
λ (Å)	0.71073	0.71073
a (Å)	26.340(3)	17.245(2)
b (Å)	13.2151(14)	16.484(1)
c (Å)	28.015(3)	16.494(1)
α (°)	90	90
β (°)	117.909(2)	109.181(1)
γ (°)	90	90
V (Å³)	8617.6(16)	4428.3(6)
Space group	*P*2₁/c	*Cc*
Z	4	4
Dcalcd (g/cm³)	1.323	1.298
μ(cm⁻¹)	6.07	5.35
R1, wR2 (I>2σ(I))	0.0995, 0.0724	0.0454, 0.0624

References cited

1) Lippard, S. J.; Berg, J. M. *Principles of Bioinorganic Chemistry;* University Science Books: Mill Valley, CA, 1994; Chapter 12.

2) a) Halpern, J. *Science* **1985**, *227*, 869-875. b) Geno, M. K.; Halpern, J. *J. Am. Chem. Soc.* **1987**, *109*, 1238-1240. c) Perutz, M. F.; Fermi, G.; Luisi, B.; Shanon, B.; Liddington, R. C. *Acc. Chem. Res.* **1987**, *20*, 309-321. d) Raphael, A. L.; Gray, H. B.

J. Am. Chem. Soc. **1991**, *113*, 1038-1040. e) Garret, T. P. J.; Glingeleffer, D. J.; Guss, J. M.; Rogers, S. J.; Freeman, H. C. *J. Biol. Chem.* **1984**, *259*, 2822-2825.

3) Schultz, B. E.; Gheller, S. F.; Muetterties, M. C.; Scott, M. J.; Holm, R. H. *Acc. Chem. Res.* **1986**, *19*, 363-370.

4) Sellmann, D.; Sutter, J. *Acc. Chem. Res.* **1997**, *30*, 460-469.

5) a) Everett, G. W.; Holm, R. H. *J. Am. Chem. Soc.* **1965**, *87*, 5266-5267. b) Cotton, F. A.; Soderberg, R. H. *J. Am. Chem. Soc.* **1962**, *84*, 872-873.

6) Stereochemical tuning of 4-coordinate structure types of cobalt(II), and the ground spin state consequences of such tuning, has been recently described: Jaynes, B. S.; Doerrer, L. H.; Liu, S.; Lippard, S. J. *Inorg. Chem.* **1995**, 34, 5735-5744.

7) a) Solomon, E. I.; Rawlings, J.; McMillin, J. R.; Stephens, P. J.; Gray, H. B. *J. Am. Chem. Soc.* **1976**, *98*, 8046-8048. b) Bertini, I.; Luchinat, C. *Acc. Chem. Res.* **1983**, *16*, 272-279. c) Bertini, I.; Lanini, G.; Luchinat, C. *J. Am. Chem. Soc.* **1983**, *105*, 5116-5118. d) Khalifah, R. G.; Rogers, J. I.; Harmon, P.; Morely, P. J.; Carroll, S. B. *Biochemistry* **1984**, *23*, 3129-3136. e) Briganti, F.; Pierattelli, R.; Scozzafava, A.; Supuran, C. T. *Eur. J. Med. Chem.* **1996**, *31*, 1001-1010.

8) Cobalt complexes supported by tris(pyrazolyl)borate ligands have been studied extensively. For recent examples, see: a) Detrich, J.; Koneèny-Vetter, W. M.; Doren, D.; Rheingold, A. L.; Theopold, K. H. *J. Am. Chem. Soc.* **1996**, *118*, 1703-1712. b) Jewson, J. D.; Liable-Sands, L. M.; Yap, G. P. A.; Rheingold, A. L.; Theopold, K. H. *Organometallics* **1999**, *18*, 300-305. c) Thyagarajan, S.; Incarvito, C. D.; Rheingold, A. L.; Theopold, K. H. *Chem. Commun.* **2001**, 2198-2199.

9) Cobalt complexes supported by tris(thioether)borate ligands have been studied recently. See: Schebler, P.; Mondimutsira, B.; Riordan, C. G.; Liable-Sands, L. M.; Incarvito, C. D.; Rheingold, A. L. *J. Am. Chem. Soc.* **2001**, *123*, 331-332.

10) a) Peters, J. C.; Feldman, J. D.; Tilley, T. D. *J. Am. Chem. Soc.* **1999**, *121*, 9871-9872. b) Barney, A. A.; Heyduk, A. F.; Nocera, D. G. *Chem. Commun.* **1999**, 2379-2380.

11) a) Benelli, C.; DiVaira, M.; Noccioli, G.; Sacconi, L. *Inorg. Chem.* **1977**, *16*, 182-187. b) Ghilardi, C.; Midollina, S.; Orlandini, A.; Sacconi, L. *Inorg. Chem.* **1980**, *19*, 301-306. c) Dapparto, P.; Midollini, S.; Orlandini, A.; Sacconi, L. *Inorg. Chem.* **1976**, *15*, 2768-2744.

12) For recent papers dealing with (triphos)Co^{2+} chemistry, see: a) Heinze, K.; Huttner, G.; Walter, O. *Eur. J. Inorg. Chem.* **1999**, 593-600. b) Heinze, K.; Huttner, G.; Schober, P. *Eur. J. Inorg. Chem.* **1998**, 183-189. c) Heinze, K.; Huttner, G.; Zsolnai, L. *Z. Naturforsch. B* **1999**, *54*, 1147-1154. d) Winterhalter, U.; Zsolnai, L.; Kirscher, P.; Heinz, K.; Huttner, G. *Eur. J. Inorg. Chem.* **2001**, 89-103. e) Rupp, R.; Huttner, G.; Kirscher, P.; Soltek, R.; Büchner, M. *Eur. J. Inorg. Chem.* **2000**, 1745-1757.

13) The abbreviation *triphos* is used herein to designate the tripodal, tridentate ligand RC(CH$_2$PPh$_2$)$_3$ (R = alkyl or aryl). This abbreviation is often used to delineate tridentate phosphines of the type PhP(CH$_2$PPh$_2$)$_2$. In this manuscript, we restrict our use of the term *triphos* to represent the former ligand class.

14) Hewertson, W.; Watson, H. R. *J. Chem. Soc.* **1962**, 1490-1494.

15) a) Lu, C. C.; Peters, J. C. *J. Am. Chem. Soc*. **2002**, *124*, 5273-5273. b) Thomas, J. C.; Peters, J. C. *J. Am. Chem. Soc*. **2001**, *123*, 5100-5101. c) Jenkins, D. M.; Betley, T. A.; Peters, J. C. *J. Am. Chem. Soc*. **2002**, *124*, 11238-11239. Also see Chapter 5.

16) Shapiro, I. R.; Jenkins, D. M.; Thomas, J. C.; Day, M. W.; Peters, J. C. *Chem. Commun*. **2001**, 2152-2153. Also see Chapter 2.

17) For a lucid discussion of cobalt(II) EPR spectroscopy, see: Bencini, A.; Gatteschi, D. *Trans. Metal Chem.* **1982**, *8*, 97-119.

18) A thorough discussion of the electronic structure of cobalt(II) systems in four-, five-, and six-coordinate geometries has been provided by Lever: Lever, A. B. P. *Inorganic Electronic Spectroscopy*, 2nd ed.; Elsevier: New York, 1984; pp 480-505.

19) a) Sacconi, L.; Midollini, S. *J. Chem. Soc., Dalton. Trans*. **1972**, 1213-1216. b) Dapporto, P.; Midollini, S.; Sacconi, L. *Inorg. Chem*. **1975**, *14*, 1643-1650. c) Mealli, C.; Midollini, S.; Sacconi, L. *Inorg. Chem*. **1975**, *14*, 2513-2521. d) Ghilardi, C. A.; Midollini, S.; Sacconi, L. *J. Organomet. Chem*. **1980**, *186*, 279-287.

20) Heinze, K.; Huttner, G.; Zsolnai, L.; Schober, P. *Inorg. Chem*. **1997**, *36*, 5457-5469.

21) Complex **3.1** contained two crystallographically independent molecules in the asymmetric unit. For brevity, only one of the molecules is explicitly discussed in the text.

22) Reinaud, O.; Rheingold, A.; Theopold, K. *Inorg. Chem.* **1994**, *33*, 2306-2308.

23) For a discussion of high spin [Tt$^{tert\text{-}butyl}$]CoCl see: Schebler, P.; Riordan, C.; Guzei, I.; Rheingold, A. *Inorg. Chem.* **1998**, *37*, 4754-4755.

24) Casey, A. T.; Mitra, S. *Theory and Application of Molecular Paramagnetism* (Bourduaux, E. A., Mulay, N. L., Eds.); Wiley: New York, 1976.

25) Cotton, F. A.; Wilkinson, G. *Advanced Inorganic Chemistry*, 5th ed.; Wiley: New York, 1988; p 729.

26) For relevant references that deal with four-coordinate cobalt(II) in approximate C_3 or C_{3v} symmetry, see the following: a) Garrett, B. B.; Goedken, V. L.; Quagliano, J. V. *J. Am. Chem. Soc.* **1970**, *92*, 489-493. b) Bertini, I.; Gatteschi, D.; Mani, F. *Inorg. Chim. Acta* **1973**, *7*, 717-720. c) Gerloch, M.; Hanton, L. R. *Inorg. Chem.* **1980**, *19*, 1692-1698. d) Gerloch, M.; Manning, M. R. *Inorg. Chem.* **1981**, *20*, 1051-1056. e) Banci, L.; Benelli, C.; Gatteschi, D.; Mani, F. *Inorg. Chem.* **1982**, *21*, 1133-1136.

27) Kahn, O. *Molecular Magnetism*; VCH Publishers: New York, 1993; pp 1-10.

28) a) Sur, S. K. *J. Magn. Reson.* **1989**, *82*, 169-173. b) Evans, D. F. *J. Chem. Soc.* **1959**, 2003-2005.

29) a) Sinn, E. *Coord. Chem. Rev.* **1970**, *5*, 313-347, and references therein. b) Ball, P. W. *Coord. Chem. Rev.* **1969**, *4*, 361-383. c) Kato, M.; Jonassen, H. B.; Fanning, J. C. *Chem. Rev.* **1964**, *64*, 99-128.

30) Ghilardi, C. A.; Mealli, C.; Midollini, S.; Nefedov, V. I.; Orlandini, A.; Sacconi, L. *Inorg. Chem.* **1980**, *19*, 2454-2462.

31) Note that the solution susceptibilities for **3.2** and **3.3** are calculated by the Evans method assuming a *monomeric* formulation for each complex.

32) Sealy, R.; Hyde, J. S.; Antholine, W. E. *Modern Physical Methods in Biochemistry* (Neuberger, A., Van Deenen, L. L. M., Eds.); Elsevier: New York, 1985; p 69.

33) Superhyperfine coupling to phosphorous in a five-coordinate cobalt(II) phosphine complex has been treated previously. See: Stelzer, O.; Sheldrick, W. S.; Subramanian, J. *J. Chem. Soc., Dalton Trans.* **1976**, 966-970.

34) a) Pilbrow, J. R. *Transition Ion Electron Paramagnetic Resonance*; Clarendon Press: Oxford, 1990. b) Aasa, R.; Vänngård, T. *J. Magn. Resonance* **1975**, *19*, 308-315.

35) Gatteschi, D. *J. Mol. Catal.* **1985**, *23*, 145-150.

36) Osmometric measurements to determine the solution molecular weights of **3.2** and **3.3** by the method of Signer were vitiated due to the tendency of these species to precipitate from toluene and benzene solution at moderate concentrations.

37) Sacconi, L.; Ciampolini, M.; Speroni, C. P. *Inorg. Chem.* **1965**, *4*, 1116-1119.

38) Nicolini, M.; Pecile, C.; Turco, A. *J. Am. Chem. Soc.* **1965**, *87*, 2379-2384.

39) Orgel, L. E. *An Introduction to Transition-Metal Chemistry*; Wiley: New York, 1960; p 174.

40) Swalen, J. D.; Gladney, H. M. *IBM J. Res. Dev.* **1964**, *8*, 515-526.

41) van Veen, G. *J. Magn. Resonance* **1978**, *30*, 91-109.

42) Jazdzewski, B. A.; Holland, P. L.; Pink, M.; Young, V. G.; Spencer, D. J. E.; Tolman, W. B. *Inorg. Chem.* **2001**, *40*, 6097-6107.